Deep-Sea Research Part I xxx (xxxx) xxx–xxx

Contents lists available at ScienceDirect

Deep-Sea Research Part I

journal homepage: www.elsevier.com/locate/dsri

Contourite depositional systems along the Mozambique channel: The interplay between bottom currents and sedimentary processes

Antoine Thiéblemont[a,b,*], F. Javier Hernández-Molina[a], Elda Miramontes[c], François Raisson[b], Pierrick Penven[d]

[a] Department of Earth Sciences, Royal Holloway, University of London, Egham, Surrey, TW20 0EX, UK
[b] TOTAL, R&D Frontier Exploration Program, Avenue Larribau, Pau, 64000, France
[c] UMR 6538 CNRS-UBO, IUEM, Laboratoire Géosciences Océan, Plouzané, 29280, France
[d] UMR 6523 CNRS, IFREMER, IRD, UBO, Laboratoire d'Océanographie Physique et Spatiale, Plouzané, 29280, France

ARTICLE INFO

Keywords:
Contourites
Bottom currents
Sedimentary processes
Water mass interfaces
Continental margin
Mozambique channel

ABSTRACT

We present a combined study of the geomorphology, sedimentology, and physical oceanography of the Mozambique Channel to evaluate the role of bottom currents in shaping the Mozambican continental margin and adjacent Durban basin. Analysis of 2D multichannel seismic reflection profiles and bathymetric features revealed major contourite deposits with erosive (abraded surfaces, contourite channels, moats, furrows and scours), depositional (plastered and elongated-mounded drifts, sedimentary waves), and mixed (terraces) features, which were then used to construct a morpho-sedimentary map of the study area. Hydrographic data and hydrodynamic modelling provide new insights into the distribution of water masses, bottom current circulation and associated processes (e.g., eddies, internal waves, etc.) occurring along the Mozambican slope, base-of-slope and basin floor. Results from this work represent a novel deep-sea sedimentation model for the Mozambican continental margin and adjacent Durban basin. This model shows 1) how bottom circulation of water masses and associated sedimentary processes shape the continental margin, 2) how interface positions of water-masses with contrasting densities (i.e., internal waves) sculpt terraces along the slope at a regional scale, and 3) how morphologic obstacles (seamounts, Mozambique Ridge, etc.) play an essential role in local water mass behaviours and dynamics. Further analysis of similar areas can expand understanding of the global role of bottom currents in deep-sea sedimentation.

1. Introduction

Contour-following currents generated by thermohaline circulation are common processes that affect continental margins and abyssal plains of the world's oceans (e.g., Stow, 1994; Faugères et al., 1999; Stow et al., 2002, 2009; Rebesco and Camerlenghi, 2008; Rebesco et al., 2014). Deposits generated by along-slope currents are known as *'contourites'* or *'contourite drifts'* (see McCave and Tucholke, 1986; Rebesco and Stow, 2001). *'Erosional features'* (e.g., abraded surfaces, contourite channels, contourite moats) are locally developed in association with contourite drifts in areas traversed by higher velocity current cores (e.g., García et al., 2009; Cattaneo et al., 2017). In some settings, *'mixed features'* develop due to long-term depositional and erosional phases that form contourite terraces (e.g., Viana et al., 2007; Hernández-Molina et al., 2009, 2017a). Other settings host interactions between along-slope (contourites) and across-slope gravity-driven processes (turbidity currents and mass transport deposits). These processes may form *'hybrid features'* (e.g., Creaser et al., 2017; Hernández-Molina et al., 2017b; Sansom, 2018). The range of depositional, erosional and mixed (erosional-depositional) features associated with a particular water mass can be interpreted as a *'Contourite Depositional System'* (CDS). Continental margins host a number of CDSs associate to a water mass within a given depth range.

Recent studies have demonstrated the effectiveness of combining oceanographic analysis and geomorphologic approaches in interpreting CDSs (e.g., western South Atlantic margin: Preu et al., 2013; Hernández-Molina et al., 2016a; Gulf of Cadiz: Hernández-Molina et al., 2016b; Mediterranean Sea: Cattaneo et al., 2017). However, CDSs can become difficult to decipher (e.g., Hernández-Molina et al., 2006a) in the case of interactions of several different water masses, intermittent oceanographic processes (e.g., eddies, internal waves), and/or complex physiography. These special cases remain less understood due to lack of

* Corresponding author. Department of Earth Sciences, Royal Holloway, University of London, Egham, Surrey, TW20 0EX, UK.
E-mail address: Antoine.Thieblemont.2016@live.rhul.ac.uk (A. Thiéblemont).

https://doi.org/10.1016/j.dsr.2019.03.012
Received 15 October 2018; Received in revised form 4 February 2019; Accepted 30 March 2019

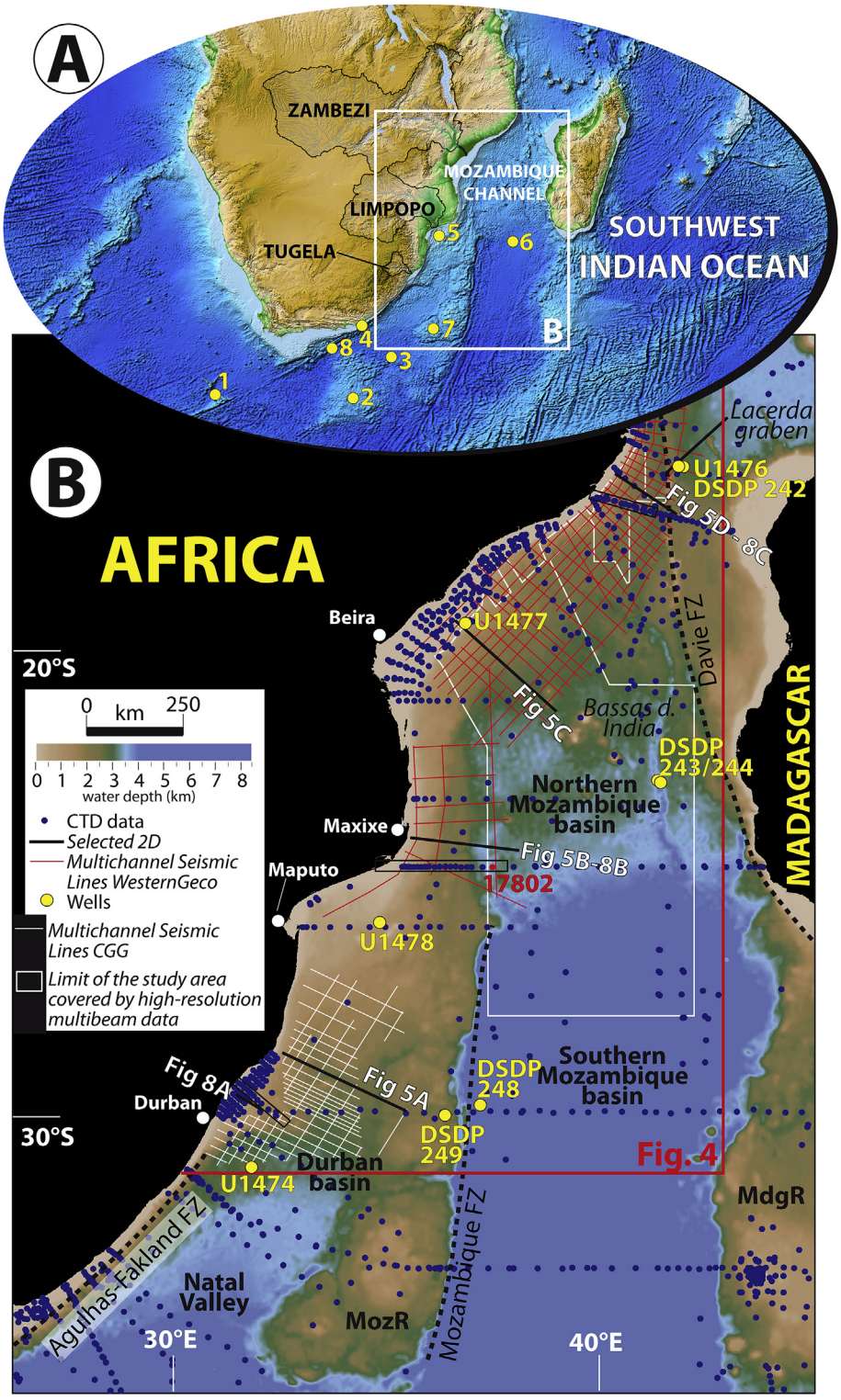

Fig. 1. Location of study area and data collection sites. (A) Bathymetric map (ETOPO1 1 arc-minute global relief model; Amante and Eakins, 2009) of the southwest Indian Ocean indicating catchment areas of the Zambezi, Limpopo, and Tugela rivers basins. Yellow dots indicate examples with large contourite deposits in present-day (or recent) ocean basins and in the ancient sedimentary record generated by bottom currents. 1: Gruetzner and Uenzelmann-Neben, 2015; 2: Uenzelmann-Neben (2001); 3: Schlüter and Uenzelmann-Neben (2008); Niemi et al. (2000); 4: Flemming (1978); 5: Preu et al. (2011); 6: Breitzke et al. (2017); Kolla et al. (1980); 7: Uenzelmann-Neben et al., 2011; 8: Uenzelmann-Neben and Huhn (2009); (B) Bathymetric map (ETOPO1 1 arc-minute global relief model; Amante and Eakins, 2009) of the Mozambique Channel indicating position of the dataset interpreted and the main bathymetric features. The study area covered by high-resolution multibeam data was interpreted based on Breitzke et al. (2017) and Wiles et al. (2017). Yellow dots show the location of the IODP Expedition 361 and DSDP Leg 25. Abbreviations: MozR = Mozambique Ridge; MdgR = Madagascar Ridge; and FZ = Fracture Zone. (For interpretation of the references to colour in this figure legend, the reader is referred to the Web version of this article.)

direct observations (Rebesco et al., 2014).

Since initial publication of studies on current-controlled sedimentation along the southern Mozambique basin (e.g., Kolla et al., 1980; 6, Fig. 1A), the southwestern region of the Indian Ocean and its CDSs have enjoyed growing scientific interest (Fig. 1A). To date, deposits directly linked to bottom current action have been described from at least eight different locations (Fig. 1A). The largest features are associated with water masses formed from Antarctic and sub-Antarctic sources. These include features along the north-eastern Agulhas Ridge and Cape Rise seamounts (Gruetzner and Uenzelmann-Neben, 2015; 1, Fig. 1A), contourite drifts of the Transkei, which include the Oribi drift, M-drift (Niemi et al., 2000; 3, Fig. 1A), and Agulhas drift (Schlüter and Uenzelmann-Neben, 2008; 3, Fig. 1A), features along the southern Mozambique Ridge (Uenzelmann-Neben et al., 2011; 7, Fig. 1A), features along the Agulhas Plateau and Passage (Uenzelmann-Neben, 2001; Uenzelmann-Neben and Huhn, 2009; 2 and 8, Fig. 1A), and features along the continental margin of Mozambique off the Limpopo River (Preu et al., 2011; 5, Fig. 1A). In summary, these studies link the

Table 1
Neutral densities used to characterize water masses interacting with bathymetric features of the Mozambique Channel based on the work of Kolla et al. (1980); Fine (1993); Toole and Warren (1993); Talley (1996); Orsia et al. (1999); Schott and McCreary (2001); DiMarco et al. (2002); Lutjeharms (2006); Ullgren et al. (2012).

Water mass	Water depth (m)	γ^n (kg/m^3)
TSW&STSW	0–200	23–25.8
SICW	200–800	26.4–26.8
AAIW	800–1500	27–27.8
RSW	900–1200	~27.4
NADW	2200–3500	> 27.8
AABW	> 4000	> 28.2

development of contourite features to particular water masses and water depth ranges. Despite the strong influence that circulation exerts on sedimentary processes (e.g., Wiles et al., 2014, 2017; Breitzke et al., 2017), long stretches of the East African continental margin have not been interpreted in terms of their depositional processes. This paper presents novel analysis of water mass influence on seafloor morphology to interpret CDSs along the East African continental margin between the latitudes of 15° S and 30° S (hereafter the Mozambique Channel). The primary aims of this work are 1) to identify the main regional sedimentary features related to bottom current action, 2) to generate a regional morpho-sedimentary map of the Mozambique Channel and 3) to interpret the interplay between sedimentary and oceanographic processes.

2. Regional setting

2.1. Geologic setting

The Mozambique Channel is located in the southwest Indian Ocean between the East African continental margin of Mozambique and Madagascar (Fig. 1A). It developed during the break-up of East Gondwana (i.e., Madagascar, India, Antarctica, and Australia) and West Gondwana (i.e., Africa and South America) (McElhinny, 1970; McKenzie and Sclater, 1971). Rifting began in the Early-Middle Jurassic (183 - 177 Ma; Eagles and König, 2008) with the opening of the northern Mozambique basin (159 Ma to 124 Ma; Jokat et al., 2003; König and Jokat, 2010; Leinweber and Jokat, 2012; Leinweber et al., 2013) and persisted to the Early Cretaceous opening of the southern Mozambique Basin (124 Ma to 84 Ma; Gradstein et al., 2012) and the Natal Valley (135 Ma to 115/90 Ma; Goodlad et al., 1982; Watkeys and Sokoutis, 1998). Currently, the Mozambique Channel consists of three major basins: the northern Mozambique basin, the southern Mozambique basin, and the Durban basin (Fig. 1B). The northern Mozambique basin is bounded by the East African continental margin of Mozambique to the west and by the Davie Fracture Zone (DFZ) to the east. The DFZ developed during southerly movement of East Gondwana (including Madagascar) (Coffin and Rabinowitz, 1987, 1992) and was later reactivated by extensional deformation (e.g., Lacerda Graben) since the late Miocene (Mougenot et al., 1986). A group of isolated carbonate platforms (e.g., Bassas Da India) formed in the middle of the northern Mozambique basin from the Paleocene to early Miocene (Courgeon et al., 2016). Late Miocene-early Pliocene cessation of carbonate deposition and initiation of graben formation along the DFZ appears to be coeval and spatially linked with the development and propagation of the East African Rift System (Franke et al., 2015). The southern Mozambique basin is bounded to the west by the Mozambique Ridge (MozR), which occurs about 100 km off the coast, and to the east by the Madagascar Ridge (MdgR) (Fig. 1B). Both ridges are interpreted to represent a large igneous province of oceanic origin (Sinha et al., 1981; Fischer et al., 2017) forming between 140 and 122 Ma for the Mozambique Ridge (König and Jokat, 2010). Finally, the Durban basin represents the eastern termination of a major east-west trending fault system, the Agulhas-Falkland Fracture Zone (Broad et al., 2006).

Open marine sedimentation began in the Early Cretaceous for the northern and southern Mozambique basins and in the Late Cretaceous for the Durban basin (Davison and Steel, 2017). Over the past 30 Ma, the areas of interest have experienced significant periods of middle Oligocene, middle Miocene, and late Pliocene hinterland uplift (Castelino et al., 2015). Periods of uplift are associated with increase in sediment transport to the adjacent basins along the southwestern Indian Ocean (Walford et al., 2005; Wiles et al., 2014; Castelino et al., 2015; Hicks and Green, 2016). Sediment delivery to the Mozambique Channel is complex and related to global eustatic changes and hinterland tectonics (Walford et al., 2005; Castelino et al., 2015; Hicks and Green, 2016; Wiles et al., 2017). Sediments are primarily sourced from the adjacent Zambezi river (present-day catchment of $1.39{\cdot}10^6$ km^2), Limpopo river (present-day catchment of $4.15{\cdot}10^5$ km^2), and Tugela river (present-day catchment of $2.91{\cdot}10^4$ km^2) (Fig. 1A). These control the general sediment type and flux delivered to the Mozambique Channel over time.

2.2. Oceanographic framework

The south Indian Ocean hosts a variety of water masses characterized by different hydrographic properties as summarized in Table 1. At present, oceanic circulation along the Mozambique Channel consists primarily of the southward flowing Mozambique current and the northward flowing Mozambique undercurrent (De Ruijter et al., 2002). The Mozambique current is part of the Agulhas current system (Lutjeharms, 2006) and is characterized by anticyclonic eddies with diameters of ~300 km (Fig. 2). Four to six anticyclonic eddies per year occur in the Channel, and propagate southwards at ~3–6 km/day (De Ruijter et al., 2002; Schouten et al., 2003; Halo et al., 2014). The Mozambique current carries Tropical Surface Water, Subtropical Surface Water (TSW and STSW, < 200 m water depth, wd), the South Indian Central Water (SICW, between 200 and 600 m wd) (De Ruijter et al., 2002), and the northwest Indian-origin Red Sea Water (RSW, 900–1200 m wd) (Donohue et al., 2000; Beal et al., 2000; Swart et al., 2010). The Mozambique and Agulhas undercurrents flow northward along the Mozambican continental slope (Fig. 2) carrying Antarctic Intermediate Water (AAIW, 800–1500 m wd) after its westward flow over the Madagascar ridge (Fine, 1993) and the North Atlantic Deep Water (NADW, 2200–3500 m wd), which flows into the Natal Valley (Toole and Warren, 1993) towards the southern Mozambique basin, south of the Mozambique Ridge. A portion of the NADW flows into the southern Mozambique basin across deep corridors within the Mozambique Ridge (Wiles et al., 2014). The upper volume of the NADW crosses a sill in the northern Mozambique basin to enter the Somali Basin, while the remaining NADW flows along the eastern boundary of the northern Mozambique basin with a southerly returning current (van Aken et al., 2004; Ullgren et al., 2012). The Antarctic Bottom Water (AABW) circulates below 4000 m wd (Fig. 2). It flows northward as a western boundary current along the southern Mozambique basin (Tucholke and Embley, 1984; Read and Pollard, 1999). Because the basin is closed in the north, the AABW is deflected to form a southerly flowing boundary current along the east flank of the southern Mozambique basin (Kolla et al., 1980).

3. Data and methods

This study utilizes bathymetry, multichannel 2D seismic reflection profiles, hydrographic data, and hydrodynamic modelling. A slope gradient map was generated using GEBCO 2014 (Weatherall et al., 2015). The bathymetric base map included data from previous works of Wiles et al. (2014, 2017) and Breitzke et al. (2017), which were used to generate the morpho-sedimentary map.

Profiles interpreted derive from a regional 2D multichannel seismic

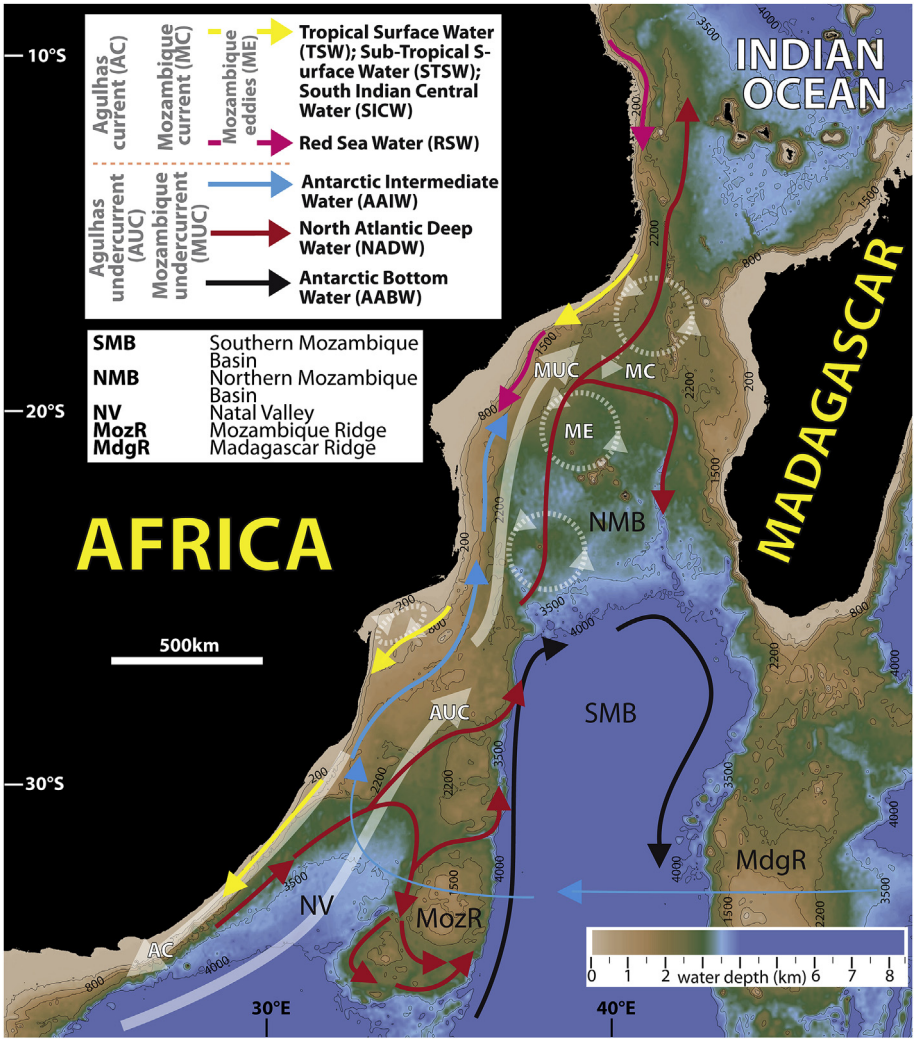

Fig. 2. Bathymetric map (ETOPO1 1 arc-minute global relief model; Amante and Eakins, 2009) of the Mozambique Channel indicating schematic position of present-day water masses.

reflection (MCSs) dataset (Fig. 1) acquired for the Mozambique basin during 2013/2014 geophysical cruises by WesternGeco. This primary dataset represents a regional grid of linear, 36179 km MCSs spaced at approximately 10–70 km intervals. Profiles were migrated in time. A second dataset was acquired for the Durban basin in 2013–2014 by CGG. The secondary dataset consists of widely spaced arrays spanning 6920 km and including 17 strike lines and 25 dip lines. The data were processed with Kirchhoff pre-stack time migration. Major morpho-sedimentary features were identified and mapped using bathymetry and seismic profiles.

Oceanographic analysis was performed using hydrographic data from the World Ocean Database 2013 (WOD13; https://www.nodc.noaa.gov/OC5/WOD13/) and a Regional Oceanic Modelling System (ROMS, version CROCO: https://www.croco-ocean.org/).

Hydrographic data from WOD13 was used to create combined hydrographic and seismic cross sections. Due to the lack of hydrographic sections, we constructed cross-slope sections by combining all available conductivity, temperature, salinity, and depth (CTD) stations and then projecting water sample stations onto the seismic cross-section at distances of up to 50 km. The cross-sections were created using Ocean Data View (Schlitzer, 2013). CTD data were also used for generating potential temperature-salinity diagrams in order to identify water masses present along the Mozambique Channel.

The Regional Oceanic Modelling System (ROMS, CROCO version), a three dimensional ocean model described by Shchepetkin and McWilliams (2005), was used to simulate the bottom currents in the Mozambique Channel. ROMS is a primitive equation model that can estimate basin-scale, regional and coastal oceanic processes at high resolution (Shchepetkin and McWilliams, 2005). ROMS uses a topography following vertical grid allowing explicit resolution of interactions between bottom topography and ocean dynamics. The model used the GEBCO 2014 (Weatherall et al., 2015) bathymetric base map smoothed for numeric constraints. The model simulation ran for 21 years (from 1993 to 2014). The model surface conditions are derived from the ERA Interim atmospheric reanalysis (Dee et al., 2011) using a bulk formulation (Fairall et al., 1996). The lateral boundary conditions are drawn from a global ocean reanalysis GLORYS (Ferry et al., 2012). To reach a high resolution 1/36° (~3 km) in the Mozambique Channel, three levels of embedded grids are used, based on the AGRIF two-way nesting method (Debreu et al., 2012). Since the mean kinematic bottom-shear-stress induced by tides affects only the shelf (i.e., Bight of Sofala; Chevane et al., 2016), barotropic tides were not introduced in the model for this simulation.

Three cross-slope hydrographic sections based on CTD stations from northern, central, and southern sector water columns were used to interpret relations between water mass stratification and sedimentary features along the continental margin. Combining these sections with potential salinity-temperature-oxygen diagrams from the same dataset allowed us to identify the main water masses in each physiographic domain. This approach also revealed lateral variation in water

mass dynamics along the Mozambique Channel. Accurate identification of water masses and their spatial correlation with seafloor morphology can elucidate longer-term oceanographic and sedimentary processes (Hernández-Molina et al., 2016a). Calculated as the oscillation frequency of a parcel displaced vertically in a statically stable environment, the buoyancy or Brunt-Väisälä frequency (N) provides information on water column stratification (Da Silva et al., 2009). It is calculated from hydrographic data (World Ocean Database, 2013) as:

$$N = \sqrt{\frac{g}{\rho}\frac{\partial \rho}{\partial z}} \quad (1)$$

where g is the gravitational acceleration, ρ is the density, and $\frac{\partial \rho}{\partial z}$ is the vertical density gradient.

This analytical approach identified numerous bottom current-controlled depositional and erosional features. We use the term *'contourites'* for sediments deposited or substantially reworked by the persistent action of bottom currents (Faugères and Stow, 2008). This term includes a large variety of sediments affected by different types of currents (Rebesco et al., 2014). Thick, extensive sedimentary accumulations are defined as *'contourite drifts'* or *'drifts'*. Interpretation of features followed criteria for drift morphology and internal configuration detailed in McCave and Tucholke (1986), Faugères et al. (1999), Rebesco and Stow (2001), Rebesco (2005), and Rebesco et al. (2014).

4. Results

4.1. Physiography of the study area

The Mozambique Channel includes three major physiographic provinces, as defined by IHO and IOC (1983): the continental shelf, the continental slope and the abyssal plain (Fig. 3). All three margin provinces were interpreted from southern, central, and northern sectors of the study area. These represent the Tugela, Limpopo, and Zambezi Rivers discharge areas, respectively (Fig. 1A).

The continental shelf exhibits an average gradient of 0.4°. It is particularly narrow (~2–15 km in width) compared to the global average of ~50 km (Shepard, 1963), except in the regions in front of the Tugela, Limpopo and Zambezi rivers (i.e., 51 km, 80 km and 130 km respectively) (Fig. 3). The continental slope is bordered to the west by the shelf-break, which is around 50–120 m water depths (set at ~200 m wd in this study). In the study area, the continental slope exhibits a relatively gentle gradient (1.1° on average) relative to the global average slope (3°, Kennett, 1982). The slope divides into upper, middle, and lower subdomains. Each subdomain was defined to highlight zones of abrupt changes in seabed gradient (Fig. 3 and Table 2); the upper, middle and lower slope, respectively, have an average gradient of: 1.6°, 1.1° and 0.9°, and occur between isobaths of: 200–1000 m, 1000–1600 m, and 1600–2400 m. The morphological seafloor changes that determine the upper, middle and lower slope subdomains roughly coincide with the distribution of large-scale flatter areas or terraces. These terraces have been described and locally characterized by Martin (1981) in the central sector: the Inharrime terrace (< 800 m wd) and the Central terrace (~1400–2000 m wd), which are separated by the SW-NE rough topography of the Almirante Leite Bank. Furthermore, a broad (~90 km) gently seaward dipping (0.3°) terrace occurs around 21° S (1300–1600 m wd) that has been described by Wiles et al. (2017) (Fig. 3). In this study, the base-of-slope is set at 2400 m water depth (wd). In areas where the buried Beira High and the Mozambique Ridge abut the continental slope (i.e., 21° S to 29° S), a steep surface (2–10°) develops at the foot of the lower slope (from ~2400 m wd) (Fig. 3). In this study, this feature belongs to the abyssal plain province.

The abyssal plain of the southern sector (i.e., Natal Valley) lies between 2400 m (uppermost, narrowest part) and ~3000 m wd (southward at ~31° S). This feature is bounded to the east by the Mozambique Ridge, which rises to a depth of 1800 m (Fig. 3). The Mozambique Ridge deepens along E-W oriented pathways (at depths of ~2000–3000 m wd) connecting the abyssal plain regions of the Natal Valley and the southern Mozambique basin. The abyssal plain depth of the Mozambique basin in the northern and central sector increases from ~2400 m to ~4000 m wd southward at ~27° S. The large-scale morphology of the abyssal plain includes numerous seamounts (i.e., Bassas Da India and Boucart) (Fig. 3).

4.2. Gravitational features

The continental slope of the southern sector hosts numerous submarine canyons extending from the upper slope to the distal limit of the lower slope. Northward (and south of the Tugela canyon), submarine canyons only occur within the lower slope (Fig. 4). Tugela canyon obliquely crosscuts the continental slope and feeds the Tugela Cone, a deep-water fan complex (Fig. 4). The canyon reaches widths of up to 19 km and incision depths of up to 1000 m in the middle slope. The canyon lacks any form of connection with the modern fluvial system. A second, unnamed canyon originates at 1400 m wd north of the Tugela canyon. It widens and deepens downslope to 2320 m wd with incision depths of up to 250 m around a prominent basement high, the Naudé Ridge (Dingle et al., 1987) (Figs. 4 and 5A). The continental slope of the central sector is dominated by along-slope sedimentary processes (Figs. 4 and 5B), except south of 27° S, where the upper slope is dissected by several submarine canyons of varying size (from 50 to 300 m wide and 10–40 m deep to 750–2000 m wide and > 400 m deep) (Fig. 4). Evidence of down-slope sedimentary processes is common along the slope of the northern sector. Large Mass Transport Deposits (MTDs) appear in the middle to lower slope, where huge deposits gather on the seafloor (Fig. 4) or appear as buried features in seismic profiles (Fig. 5C). This sector also hosts many submarine canyon systems (SCSs). Wiles et al. (2017) identified three different SCSs of this area. From north to south, these include the Angoche SCS, the Middle Zambezi SCS, and the Lower Zambezi SCS (Fig. 4). In the Angoche SCS, the margin consists of a series of canyons that extend across the shelf towards the lower slope and from the shelf to the middle slope (Fig. 4). These canyons reach widths of up to 4 km (Fig. 5D). The Lower Zambezi SCS consists of canyons mostly initiating in the middle slope at around 1000 m wd. A few of these canyons appear at around 300 m wd. These canyons can reach 12 km in width (Fig. 5C). Along the abyssal plain, sedimentary lobes form at the distal limit of the lower slope of the Angoche SCS and the Lower Zambezi SCS (Figs. 4, 5C and 5D). The Middle Zambezi SCS consists of canyons mostly initiating in the middle slope (Fig. 4). The present-day canyons lack any form of connection either with modern continental drainage channels or with incisional canyons on the shelf. These canyons reach widths of up to 7 km and incision depths of up to 200 m at around 2500 m wd. Along the abyssal plain, the Middle Zambezi SCS converges at about 19° S to join the Zambezi Valley. The combined feature then flows towards the south confined by the western flank of the Davie Fracture Zone (DFZ) until about 25° S where a large sedimentary lobe develops (Fig. 4).

4.3. Contourite features

Our analysis identified a wide range of contourite features, including depositional (drifts and sedimentary waves), erosional (abraded surfaces, moats, channels, scours, and furrows), and mixed (contourite terraces) features occurring from the shelf break to the abyssal plain (Fig. 4). Contourite drifts represent important along-slope accumulations of sediment that appear as continuous, layered seismic reflections with internal, regional-scale unconformities (Fig. 6). Erosional features are mainly characterized by truncated reflections underlying stratified and/or chaotic facies. These generally show relatively high amplitude reflections (HARs) relative to those representing associated drifts (Fig. 6). The mixed features (contourite terraces) display similar seismic facies defined by continuous to discontinuous, subparallel, and

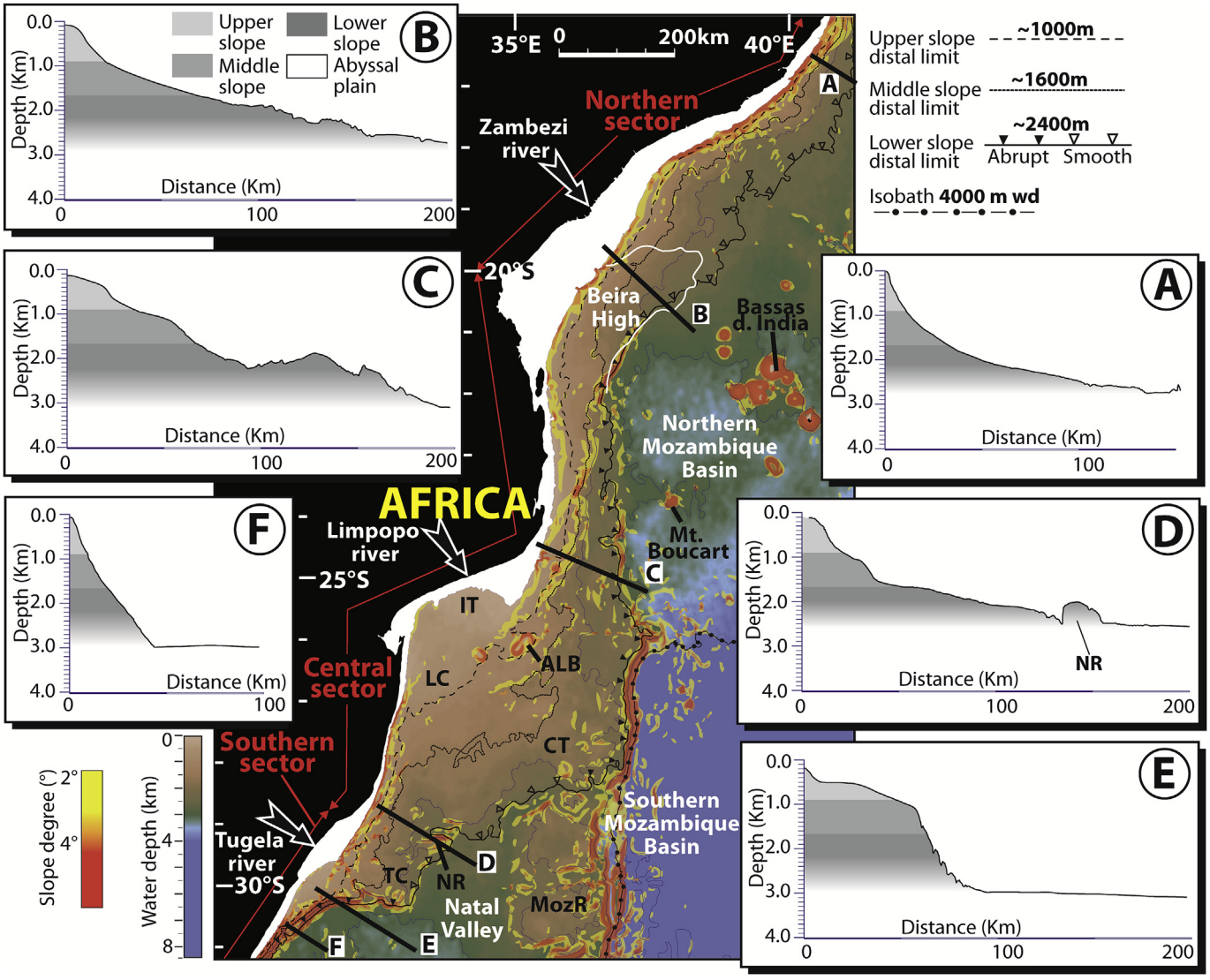

Fig. 3. Slope gradient map for surfaces dipping ≥2° along the Mozambican continental margin. Bathymetric map includes the main physiographic domains (continental shelf; upper, middle, and lower continental slopes; and abyssal plain) and morphological features superimposed (ETOPO1 1 arc-minute global relief model; Amante and Eakins, 2009). The white line indicates the location of the buried Beira High. Abbreviations: ALB = Almirante Leite Bank; CT = Central Terrace; IT = Inharrime Terrace; LC = Limpopo Cone; MozR = Mozambique Ridge; NR = Naudé Ridge; and TC = Tugela Cone. (A) To (F) Bathymetric profiles showing seafloor morphology for the three different sectors: (A) and (B) are the northern sector, (C) and (D) the central sector, and (E) and (F) the southern sector.

occasionally truncated seismic reflections (Fig. 6). High amplitude reflections are generally found along these terraces with a number of 2D sedimentary waves (e.g., Flemming, 1978; Green, 2011).

4.3.1. Depositional contourite features

Drifts are the dominant depositional features observed. The largest of these features are *'plastered drifts'* and *'elongated-mounded drifts'*. Large, plastered drifts of the Mozambique continental slope show a

Table 2
Morphological characteristics (shape, gradient and width) for the continental slope subdomains (upper, middle and lower slopes) of the southern, central and northern sectors within the study area. Letters (A-F) correspond to bathymetric profiles shown in Fig. 3.

	Continental slope								
	Upper Slope			*Middle Slope*			*Lower Slope*		
	Sectors			**Sectors**			**Sectors**		
	Southern	**Central**	**Northern**	**Southern**	**Central**	**Northern**	**Southern**	**Central**	**Northern**
Shape	Concave (F)/ convex (E)	Convex (C,D)	Convex (B)/ concave (A)	Concave (F)/ convex (E)	Convex (C, D)	Concave (A, B)	Concave (E, F)	Convex (C, D)	Concave (A, B)
Gradient[a] (degrees)	7.2°/1.5°	1°	2.6°/3.7°	4.7°/1.4°	0.9°	1.4°	1.3°	1.1°	0.8°
Width[a] (km)	~4/~56	~20 to 45	~25/~10	~6/~82	~10 to 90	~15 to 50	~10	~10 to 70	~70 to 170

[a] Represents average data.

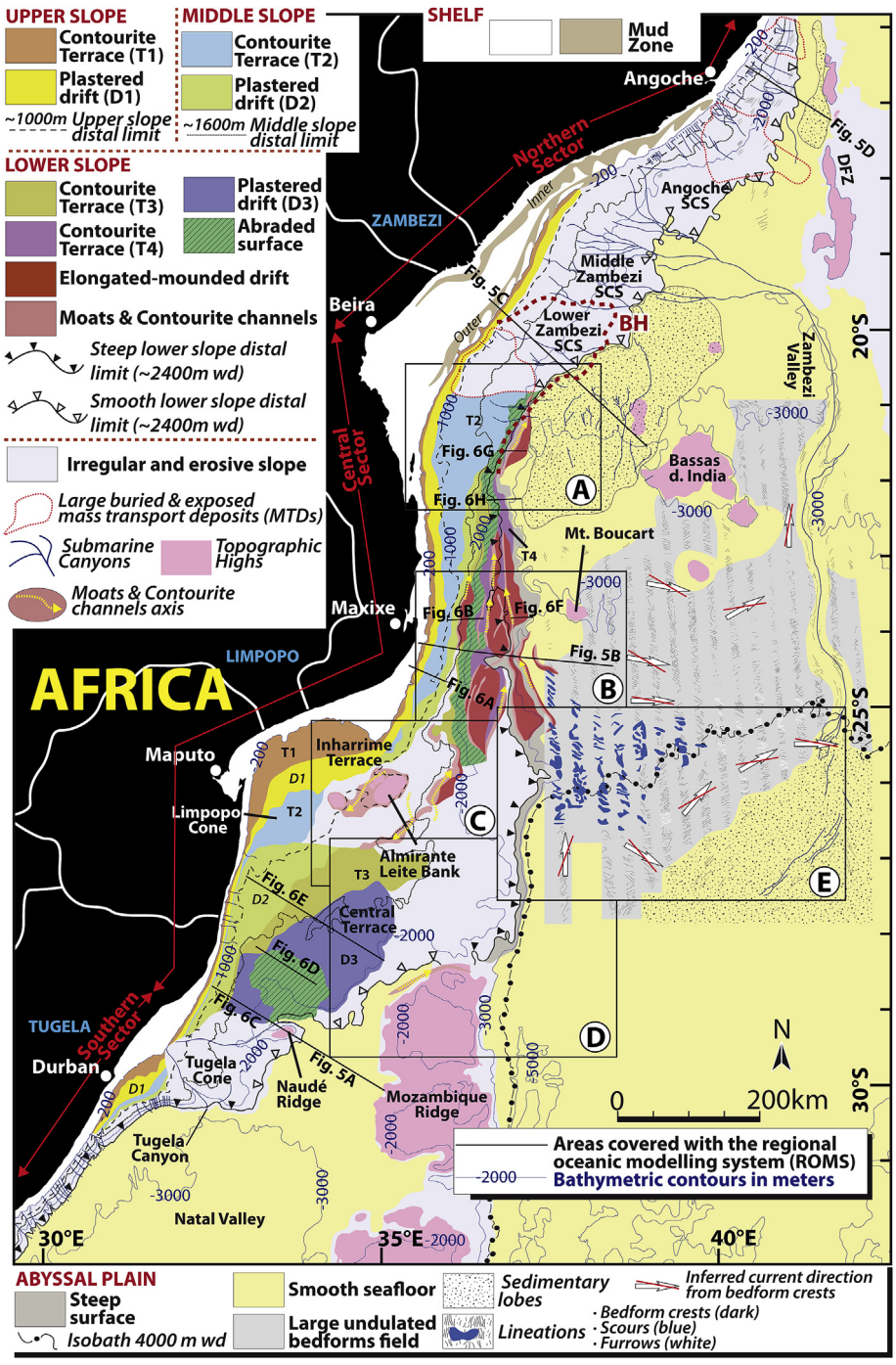

Fig. 4. Morpho-sedimentary map of the Mozambique Channel. This map illustrates the complex morphology of the Mozambique Channel as well as the interplay between down- and along-slope processes. Contourite depositional, erosional, and mixed erosive-depositional features are indicated. Lineations based on Breitzke et al. (2017) and submarine canyons based on Wiles et al. (2017). Abbreviations: DFZ = Davie Fracture Zone and SCS = Submarine Canyon Systems.

prominent along-slope trend (Fig. 4). Elongated-mounded drifts are dispersed throughout the continental slope and abyssal plain of Mozambique's central sector (Fig. 4). In addition to large-scale plastered and elongated-mounded drifts, other minor depositional features include large *'sedimentary waves'* previously described by Breitzke et al. (2017). These exhibit a wavy geometry (Fig. 5B) and occur throughout the abyssal plain, particularly south of the Bassas Da India seamounts in the centre of the Mozambique Channel (Fig. 4).

The three plastered drifts recognized in this study were informally referred to as D1 to D3 based on their water depth range along the slope (D1 being the shallowest and D3 the deepest; Fig. 4). *'Plastered drifts 1 and 2'* (D1 and D2) are located between ~300 and 600 m wd along the upper slope and between ~900 and 1300 m wd along the middle slope, respectively (Fig. 4). These show aggradational and progradational internal reflection configurations with thickness variations that indicate depocenters parallel to the slope (Figs. 5E, 6A and 6B, and 6I). In the southern sector, the 10–40 km wide D1 developed between 30° S and the Tugela Cone (Fig. 4). In the central sector, D1 spans about 20 km width and extends ~56 km along the Inharrime Terrace (Fig. 4). In the northern sector, D1 is about 7 km wide and disappears near 18° S (Fig. 4). In the southern sector, the 15 km wide D2 developed between 30° S and the Tugela Cone (Fig. 4). In the central sector, between 29° S

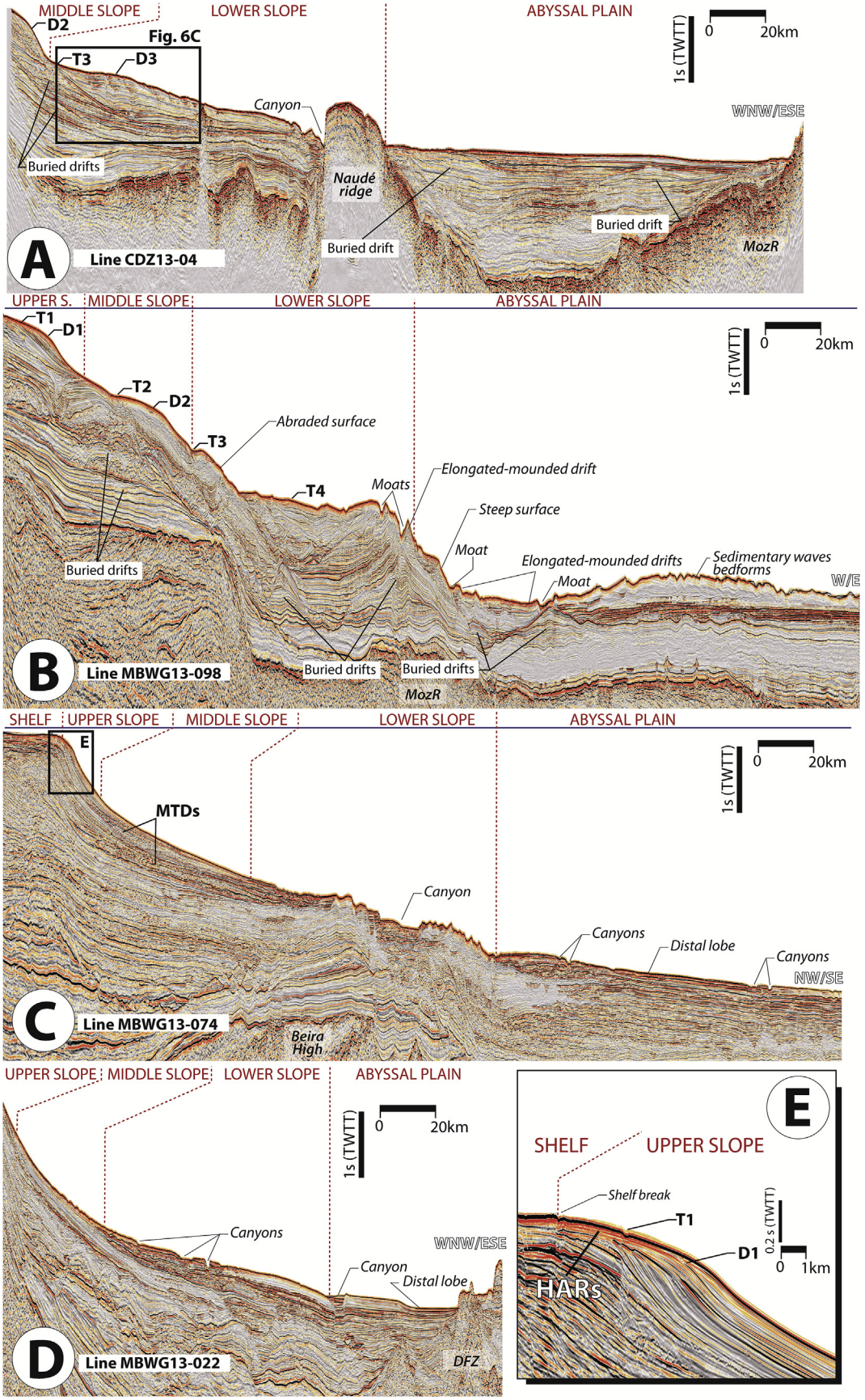

Fig. 5. Examples of four multichannel seismic reflection profiles of the Mozambican continental margin from south (A) to north (D), showing the major morpho-sedimentary features. Horizontal scale is the same for all the profiles. (E) Inlay illustrating the D1 drift and the T1 terrace, as well as high amplitude reflection patterns (HARs) of contourite terrace T1. Location in Figs. 1 and 4 (section (A) courtesy of CGG Multi-client and New Ventures and sections (B, C), and (D) courtesy of INP and WesternGeco Multiclient).

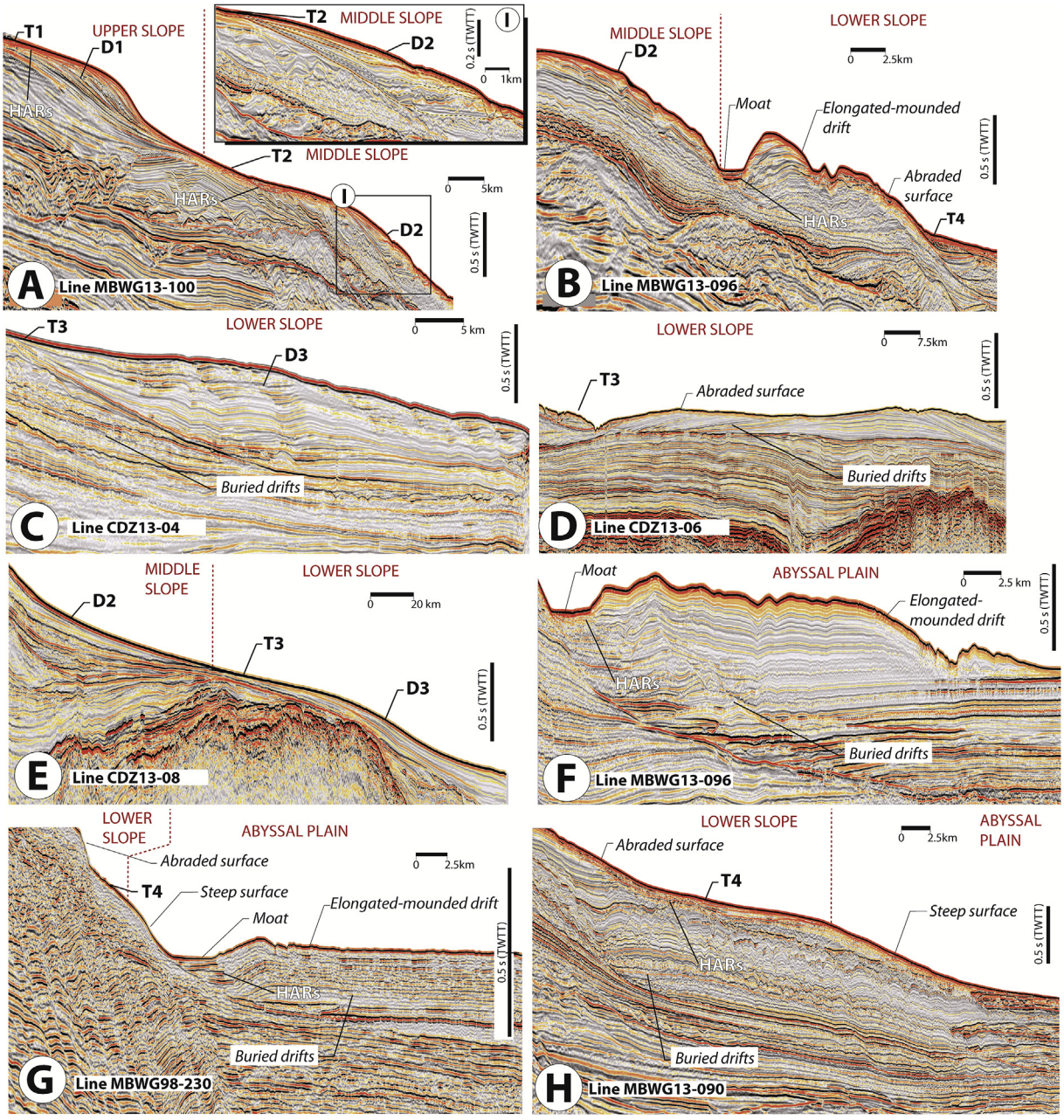

Fig. 6. Examples of depositional, erosional, and mixed contourite features from multichannel seismic reflection profiles. Details of contourite terraces T1 and T2 in (A), T3 in (C), (D), and (E), and T4 in (G) and (H). Examples of plastered drift D1 are illustrated in (A), D2 in (A), (B), and (E), and D3 in (C) and (E). Moats and elongated-mounded drifts are shown in (B), (F), and (G). Abraded surfaces and steep surfaces are illustrated in (B), (D), (G), and (H). (I) Inlay illustrating the sedimentary stacking pattern of plastered drift D2. Locations in Fig. 4 for (A–H), in Fig. 11 for (A, B, E, F, G) and (H). Abbreviation: HARs = High Amplitude Reflections. Profiles (A, B, F, G) and (H) courtesy of INP and WesternGeco Multiclient. Profiles (C–E) courtesy of CGG Multi-client and New Ventures.

and 25° S, D2 spans about 10 km in width (Fig. 4), and extends ~116 km near 27° S before it disappears in the vicinity of topographic highs associated with the Almirante Leite Bank (Fig. 4). North of the Almirante Leite Bank, D2 is about 6–30 km wide and disappears in the vicinity of the southeastern limb of the Beira High, near the northern sector (Fig. 4). The deeper *'plastered drift 3'* (D3) occurs in the lower slope of the central sector (between ~27° S and 29° S) at ~1500–2200 m wd (Fig. 4). Between the Tugela Cone and the abraded surface, D3 extends to 88 km width (Fig. 4). In this area, D3 exhibits aggradational to progradational internal reflections with a more pronounced upslope progradational stacking pattern than those exhibited by drifts D1 and D2 (Fig. 6C). North of the abraded surface, D3 extends to a width of about 110 km along the Central Terrace (Fig. 4) and exhibits predominantly progradational and seaward internal reflections (Fig. 6E).

Apart of the aforementioned plastered drifts D1 to D3, the central sector hosts other *'elongated-mounded drifts'* (Fig. 4). Along the distal limit of the middle slope, elongated-mounded drifts occur east of the Almirante Leite Bank, near 24° S (Fig. 4), where they reach about 12 km in width (Fig. 6B). Along the lower slope, elongated-mounded drifts are widespread from 22° S to 26° S, ranging 1–20 km in width (Fig. 4). From the distal limit of the lower slope to about 3200 m wd, elongated-mounded drifts occur in association with steep surfaces of the Mozambique Ridge (29° S to 22° S) and the south-eastern limb of the Beira High (21° S). These drifts reach widths of about 6–60 km (Figs. 4, 5B and 6F, and 6G).

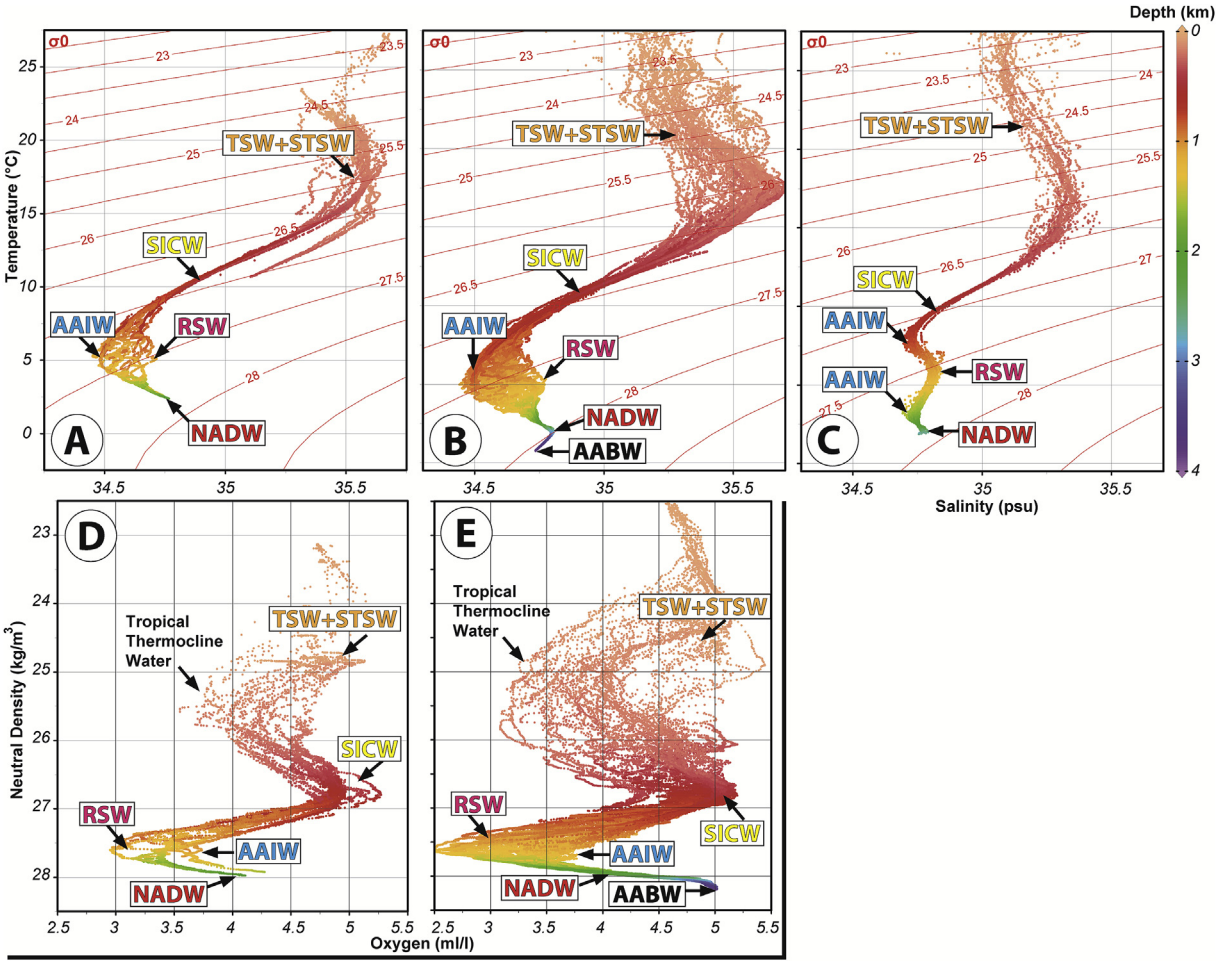

Fig. 7. (A–C) Temperature (°C) vs. Salinity (psu) diagrams for southern, central, and northern sectors respectively. (D–E) Panel plots with neutral densities (kg/m^3) vs. Oxygen content (ml/l) along the Mozambican continental margin for data collected from hydrographic sections of the southern (D) and central (E) sectors. Deep water mass circulation denoted as: AABW = Antarctic Bottom Water; NADW = North Atlantic Deep Water; AAIW = Antarctic Intermediate Water; RSW = Red Sea Water; SICW = South Indian Central Water; TSW-STSW = Tropical Surface Water – Subtropical Surface Water. (For interpretation of the references to colour in this figure legend, the reader is referred to the Web version of this article.)

'Sedimentary waves' occur along most of the basin floor of the central sector (Fig. 4 and 5B). At water depths of ~3500–4500 m, sedimentary waves can reach 60–80 m in height and up to 5 km in length, with wavelengths around 2.5–3 km. These features generally orient in a NE-SW direction, but then shift to WSW-ENE and WNW-ESE orientations to the north (Fig. 4). For water depths between ~3000 and 3400 m, sedimentary waves reach heights of 35–60 m, wavelengths around 1–2 km, and lengths of up to 10 km. These shallower features strike NW-SE, but shift into W-E and NE-SW orientations to the east (Fig. 4).

4.3.2. Erosional contourite features

Erosive contourite features occur locally along the Mozambican continental margin and basin floor. Erosional features include moats/contourite channels, abraded surfaces, and lineations (i.e., scours and furrows) (Fig. 4). *'Abraded surfaces'* occur along the lower slope of the central sector (Figs. 4, 5B and 6B, 6G, and 6H), and north of the Naudé Ridge (~50 km wide, ~100 km long, and deepening from ~1900–2300 m wd) (Fig. 4 and 6D). They also appear as steep surfaces related to the Mozambique Ridge (29° S to 22° S) and the southeastern limb of the Beira High (21° S) at the base of the slope (Figs. 4, 5B and 6G, and 6H). *'Moats'* are associated with elongated-mounded drifts and exhibit U-shaped cross sections (Figs. 4, 5B and 6B, 6F, and 6G). These features can span up to 3 km in width and incise to depths of up to 100 m *'Contourite channels'* develop in the vicinity of the large topographic highs of the Almirante Leite Bank and within the deeper corridor of the Mozambique Ridge (Fig. 4). *'Lineations'* (i.e., scours and furrows) occur along the abyssal plain near 26° S (Fig. 4). *'Scours'* form between 3500 and 4500 m wd. Often exhibiting a crescent-like shape (Breitzke et al., 2017), these can reach 20 km in length, 3–7 km in width and incisional depths of up to 450 m. Several large *'furrows'* (i.e., 60–100 m deep, 2–3 km wide, and 8–15 km long) are located east of the giant erosional scours between 3600 and 4300 m wd. Furrows generally assume a NW-SE or E-W orientation and a smooth V-shape morphology as described in Breitzke et al. (2017).

4.3.3. Mixed features

'Contourite terraces' represent mixed features that appear as subhorizontal elements developed during long-term depositional and erosional phases of the continental slope (Hernández-Molina et al., 2016a). These form erosive features in proximal domains and mostly depositional features in distal domains. Terraces are morphological features that extend to distinct depth intervals above large plastered drifts to produce long flatter areas with subtle (< 1°) seaward dips along the Mozambican margin (T1 to T4) (Fig. 5B and 6). Terraces develop along the upper slope (T1 at ~300 m wd) near the transition between upper and middle slopes (T2 at ~800 m wd), near the transition between middle and lower slopes (T3 at ~1500 m wd), and along the lower slope (T4 at ~2200 m wd) (Fig. 4 and 5B).

'Terrace 1' (T1) is associated with the upper surface and landward proximal domain of the D1 drift (Fig. 6A). In the southern sector, T1

develops between 30° S and the Tugela Cone to reach a width of ~4 km. In the central sector, T1 reaches ~4–5 km in width and extends ~50 km along the Inharrime Terrace. In the northern sector, T1 reaches about ~2.5 km in width and disappears near 18° S (Fig. 4). *'Terrace 2'* (T2) is associated with the top surface and landward proximal domain of the D2 drift (Fig. 6A). In the southern sector, T2 forms between 30° S and the Tugela Cone to reach widths of ~15 km. In the central sector between 29° and 25° S, T2 spans less than 1 km in width. It extends up to ~30 km near 27° S (Limpopo Cone) before it disappears in the vicinity of the topographic highs of the Almirante Leite Bank. North of the Almirante Leite Bank, T2 reaches widths of about ~20–30 km and extends 80 km near the Beira High. T2 disappears in the vicinity of the large MTDs occurring in the northern sector (Fig. 4). *'Terrace 3'* (T3) is associated with the top surface and landward proximal domain of the D3 drift (Fig. 6C and 6E). In the central sector, T3 is about ~4–25 km wide, extending ~60 km and disappearing in the vicinity of the topographic highs of the Almirante Leite Bank. North of the Almirante Leite Bank, T3 is about ~4 km wide but poorly developed relative to T1 and T2. T3 disappears in the vicinity of the southeastern limb of the Beira High (21° S) (Fig. 4). *'Terrace 4'* (T4) only appears from 21° to 25° S where it spans about ~60 km in width (Fig. 6H). Toward the northern sector, T4 is about ~2 km wide and disappears in the vicinity of the southeastern limb of the Beira High (21° S) (Fig. 4). Unlike T1-T3, which exhibit mostly a depositional character in their distal domain (i.e., plastered drifts D1 to D3), T4 exhibits a steep surface with an erosive character along its seaward flank (Fig. 4 and 6H).

4.4. Identification of water masses and associated oceanographic processes

Temperature and salinity profiles indicate seven major water masses operating the Mozambique Channel of the southwest Indian Ocean (Fig. 7 and Table 1). These include three of Indian origin (TSW, Tropical Surface Water; STSW, Subtropical Surface Water; and SICW, South Indian Central Water), one of North Atlantic origin (NADW, North Atlantic Deep Water), one of Red Sea origin (RSW, Red Sea Water), and two of Antarctic origin (AAIW, Antarctic Intermediate Water; AABW, Antarctic Bottom Water). An eighth water mass lies below the TSW, the Tropical Thermocline Water, which differs from STSW (same temperature) according to the former's much lower oxygen content (Lutjeharms, 2006) (Fig. 7D and 7E). The TSW, STSW, Tropical Thermocline Water, and SICW make up the upper water column, while the AAIW and RSW constitute the intermediate water column, and the NADW and AABW form the base of the water column (Ullgren et al., 2012). Select neutral density profiles in this region showed that γ^n = ~26.4 kg/m^3 for the Subtropical Surface Water (STSW) – South Indian Central Water (SICW) transition, γ^n = 27 kg/m^3 for the SICW – Antarctic Intermediate Water (AAIW) transition, γ^n = 27.8 kg/m^3 for the AAIW – North Atlantic Deep Water (NADW), and γ^n = 28.2 kg/m^3 for the NADW – Antarctic Bottom Water (AABW) (Toole and Warren, 1993; Talley, 1996; Ullgren et al., 2012) (Fig. 7). Identification of present water masses and their correlation with seafloor morphology can help elucidate longer-term oceanographic and sedimentary processes. The present oceanic circulation offshore of Mozambique is relatively complex and composed of various water masses interacting at different depths. These are briefly described below.

4.4.1. Identification of water masses along the southern sector

At shallow water depths (< 200 m), the Tropical Surface Water (TSW; above 24 °C) covers the Sub-Tropical Surface Water (STSW), which exhibits a maximum in salinity of 35.7 psμ and temperature of around 17 °C (Fig. 7A). Both are saturated in dissolved oxygen (Fig. 7D). Tropical Thermocline Water can be distinguished from STSW (same temperature) by the former's much lower dissolved oxygen concentrations (< 4 ml/l) (Fig. 7D). Directly below the STSW, within a neutral density range of 26.4 kg/m^3 to 26.8 kg/m^3 and a water depth range of about 200–600 m, temperature-salinity properties declined down to values of 8–14 °C and 34.8–35.5 psμ, respectively. These parameters are characteristic of the South Indian Central Water (SICW) (Fig. 7A). The relatively fresh Antarctic Intermediate Water (AAIW) and relatively saline Red Sea Water (RSW) with neutral densities ranging from 27.0 to 27.8 kg/m^3 occupy intermediate depths below the thermocline (Fig. 7A). The AAIW forms a salinity minimum of < 34.5 psμ, while the RSW modifies this minimum by interleaving the water column with relatively saline layers (> 34.6 psμ) (Fig. 7A). Further downslope, at neutral densities greater than 27.8 kg/m^3, a cold (~2 °C) and high salinity (> 34.8 psμ) bottom layer is interpreted as the North Atlantic Deep Water (NADW) (Fig. 7A).

4.4.2. Identification of water masses along the central sector

Along this hydrographic section, the TSW, STSW, and Tropical Thermocline Water occupy the upper water column (< 200 m wd, γ^n < 25.8 kg/m^3) (Fig. 7B and 7E). The TSW forms surface water, which is warmer than 24 °C. Directly beneath, the STSW exhibits a maximum in salinity of 35.8 psμ at temperatures of around 17 °C (Fig. 7B). TSW and STSW are saturated with dissolved oxygen while Tropical Thermocline Water, at the same depth as the STSW salinity maximum, exhibits lower dissolved oxygen concentrations (< 4 ml/l) (Fig. 7E). At water depths of 200–600 m, temperature-salinity properties (8–14 °C and 34.8 to 35.5 psμ, respectively) are characteristic of the SICW (26.4 kg/m^3 to 26.8 kg/m^3) (Fig. 7B). The AAIW appears at water depths of ~800 m near the neutral density of the SICW-AAIW transition (27 kg/m^3) (Fig. 7B). The AAIW layer at this section exhibits low salinities (~34.5). AAIW combines high salinities (> 34.6 psμ) and low dissolved oxygen (< 3.5 ml/l) layers of the RSW at water depths of 800 and 1500 m (Fig. 7B and 7E). Below, as neutral densities surpass 27.8 kg/m^3, the NADW (< 4 °C, ~34.8 psμ) appears at around 2200 m wd (Fig. 7B). At water depths around 3500–4000 m, cold (~1.5 °C), low salinity (< 34.7 psμ) bottom waters approach the neutral density of the NADW-AABW transition (28.2 kg/m^3) (Fig. 7B).

4.4.3. Identification of water masses along the northern sector

The hydrographic section located in the northern part of the margin intersects the 2000 m isobath. Dissolved oxygen data for this part of the basin was not available. The surface water column is characterized by warm temperatures (> 24 °C) and high salinity (~35.2 psμ) of the TSW (Fig. 7C). Beneath this water mass lies the STSW, which exhibits a maximum salinity of ~35.5 psμ and temperature of 15 °C to give a neutral density of < 25.8 kg/m^3 for its upper layers (< 200 m wd) (Fig. 7C). Below the STSW salinity maximum, temperature-salinity properties increase to values characteristic of the SICW, which exhibits a neutral density range of 26.4 kg/m^3 to 26.8 kg/m^3 in the 200–600 m depth range (Fig. 7C). The base of the SICW reaches a local salinity minimum and neutral density of 27 kg/m^3, which marks the transition to properties associated with intermediate water masses (Fig. 7C). The intermediate water masses exhibit a neutral density range of 27 kg/m^3 to 27.8 kg/m^3 and flow at depths of 800–1500 m wd. The water masses are relatively salty and salinities greater than 34.9 psμ in the middle of the density range indicate the presence of the RSW (Fig. 7C). Below the RSW, salinities decrease (< 34.7 psμ) to another local minimum around 1500 m wd and 27.6 kg/m^3 density indicating a deeper AAIW core (Fig. 7C). For deeper water approaching 27.8 kg/m^3 neutral density, salinities increase to about 34.8 psμ at temperatures of around 2 °C. These parameters indicate the presence of the NADW in contact with the seafloor at around 2200 m wd (Fig. 7C).

4.4.4. Associated interface processes

Near-bottom layers for the water masses described above indicate that TSW, STSW and SICW traverse the continental shelf and upper slope of the Mozambican margin while the AAIW and RSW traverse the middle and lower slopes, and the NADW and AABW occupy the Mozambican base-of-slope and deep basins (Fig. 2 and 8). Interfaces between the TSW + STSW/SICW and SICW/AAIW (and RSW) thus

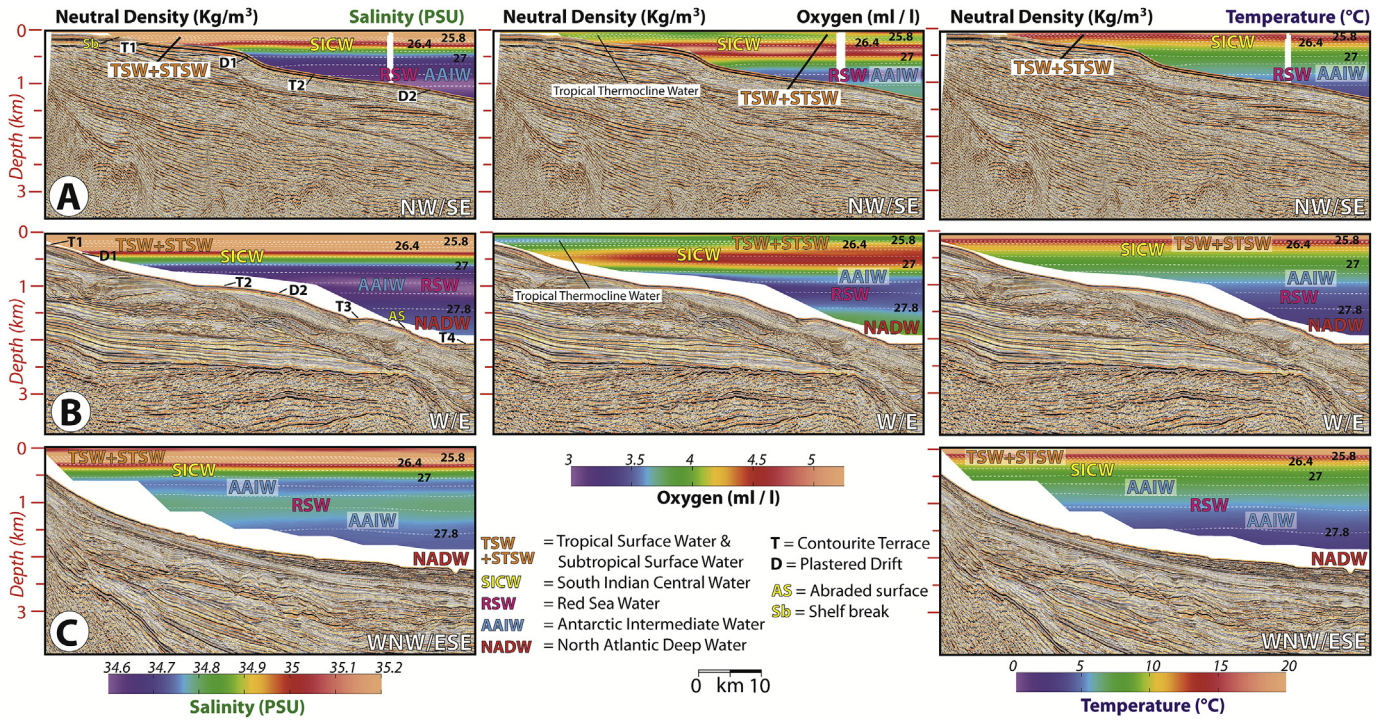

Fig. 8. Seismic and hydrographic vertical sections for the Mozambican continental margin. The water column colour ranges indicate salinity (psu), temperature (°C) and oxygen content (ml/l). These profiles are located in Fig. 1. Water mass interpretations and major contourite features are indicated on the sections. Profile (A) courtesy of TOTAL and partners and Profiles (B, C) courtesy of INP and WesternGeco Multiclient. (For interpretation of the references to colour in this figure legend, the reader is referred to the Web version of this article.)

interact with the Mozambican slope (Fig. 8), whereas interfaces between AAIW (and RSW)/NADW and NADW/AABW affect the Mozambican base-of-slope and basin floor. The interfaces (pycnoclines) between the TSW + STSW/SICW and SICW/AAIW are characterized by sharp density gradients while the interface between AAIW/NADW is characterized by a diffuse density gradient with a gradual transition from one water mass to the other (Fig. 9C). High values of buoyancy (Brunt-Väisälä) frequency (> 2 cycl/h) is observed at around 800 m wd and above ~300 m wd (Fig. 9A), matching the TSW + STSW/SICW and SICW/AAIW interfaces. Above ~300 m wd, the buoyancy (Brunt-Väisälä) frequency reaches maximum values around 50–100 m wd (> 6 cycl/h) (Fig. 9B). Internal waves (solitons) were observed propagating from the shelf of the Bight of Sofala into the Indian Ocean (20° S to 21° S; Fig. 10D and 10E). Fig. 10 (A, B, and C) also illustrates internal wave propagation towards the coast in the Bay of Maputo.

4.5. Circulation model results

Bottom current simulations carried out with the Regional Oceanic Modelling System (ROMS) indicated that currents often flow parallel to the isobaths but exhibit some degree of variation in direction and velocities depending on location (Fig. 11). Along the upper slope, the simulated bottom currents show southward movement with mean velocities of > 12.5 cm/s (Fig. 11A and 11B). The upper slope along the Inharrime Terrace and Limpopo Cone experienced W-NW transport near the shelf break (200 m wd) with inversions towards the W-SW, especially along the distal limit of the upper slope (~1000 m wd) (Fig. 11C). Flow directions corresponded to a local cyclonic eddy previously described by Lamont et al. (2010). Along the middle slope, simulated bottom currents showed greater variability in current direction. Current direction was less rectilinear and flowed northward with at relatively low current velocities (< 12.5 cm/s). By contrast, current direction indicated southward transport deflected E-SE associated with the highest estimated current velocities (> 12.5 cm/s) (Fig. 11A, C, and 11D). Higher current speeds correspond to periods of southward moving anticyclonic eddies as documented by Schouten et al. (2003). Slope morphology constrains current direction near the Almirante Leite Bank. Steeper slope flanks in this area intensify circulation (> 25 cm/s) (Fig. 11C). Along the lower slope, simulated currents showed predominantly northward transport with mean velocities reaching > 25 cm/s (Fig. 11). Faster currents occur along steep surfaces around 1800 m (Figs. 11B), 2500 m (Fig. 11A) and 3000 m wd (Fig. 11D and 11E) with mean velocities of ~12.5 cm/s but locally reaching as much 25 cm/s. Along the abyssal plain, simulated bottom currents intensify along the Mozambique Ridge with mean velocities oscillating between 12.5 and 25 cm/s (Fig. 11D) and around Mt. Boucart, especially along its western flank, where mean velocities can exceed 25 cm/s (Fig. 11B). Current directions indicate predominantly northward transport along the western side of the margin and eastward deflection in the middle of the abyssal plain (Fig. 11A and 11E).

5. Discussion

The morpho-sedimentary map and oceanographic features described above enable interpretation of sedimentary processes operating within the Mozambique Channel. Interpretation indeed suggests that bottom currents adequately explain the formation and variability of observed contourite features (depositional, erosive and mixed). Matching contourite types with the relevant bottom water masses allows us to propose a depositional model for the Mozambique Channel.

5.1. Water-mass interfaces sculpt contourite terraces

Contourite terraces 1 and 2 represent regional scale features formed along the Mozambique Channel while contourite terraces T3 and T4 show much more variation in their spatial distribution (Fig. 4). The terraces occur in water depths of ~300 m for T1, ~800 m for T2, ~1500 m for T3 and ~2200 m for T4. Hydrographic Sections A and B

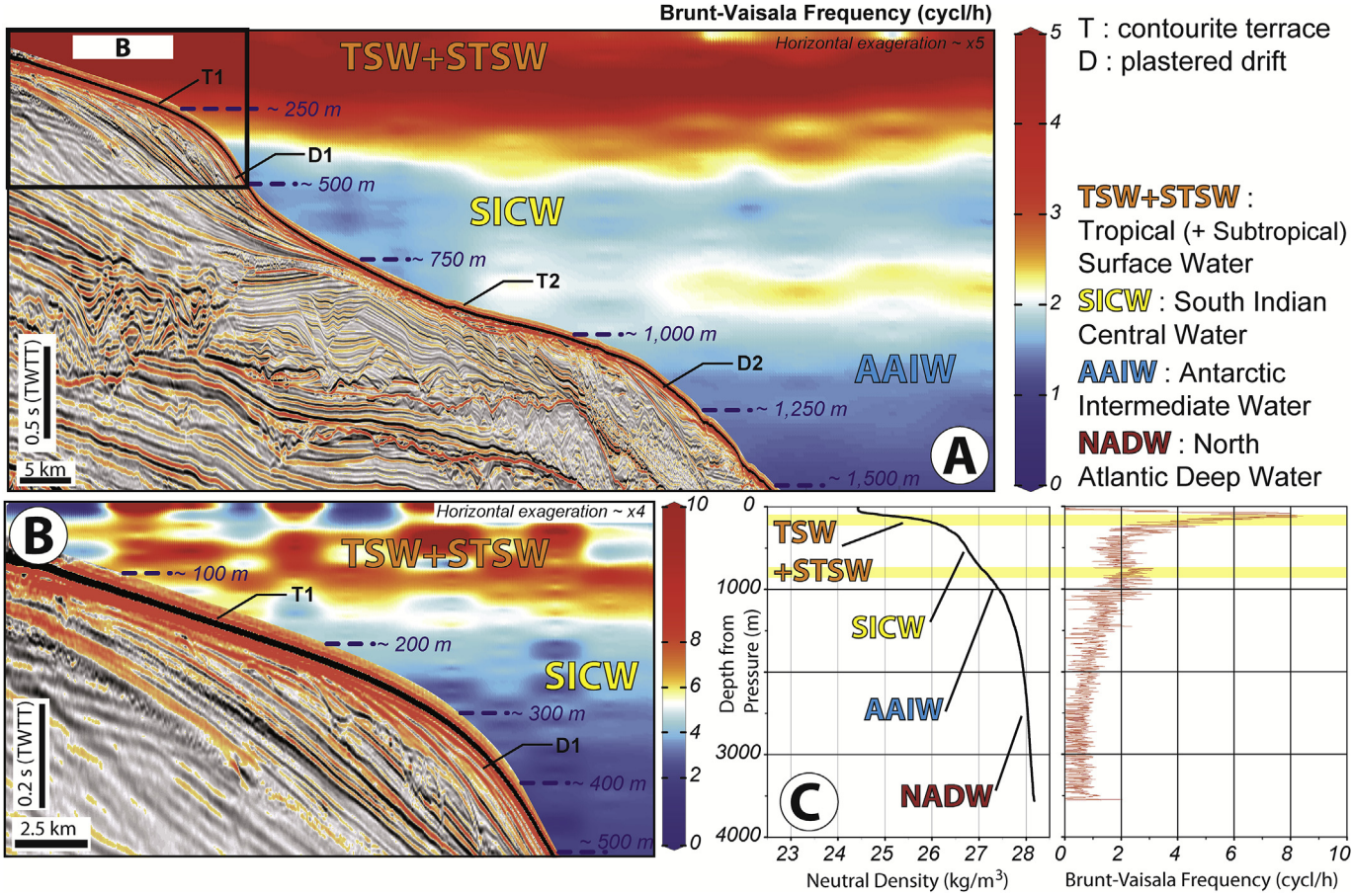

Fig. 9. (A) Seismic and hydrographic vertical section for the Mozambican continental margin. Water column colour range indicates the buoyancy (Brunt-Väisälä) frequency (cycl/h). This profile is denoted as Fig. 6A located in Fig. 4. (B) Inlay illustrating the buoyancy (Brunt-Väisälä) frequency (cycl/h) along contourite terrace T1. Seismic line courtesy of INP and WesternGeco Multiclient. (C) Panel plots with Depth from pressure (m) vs. Neutral densities (kg/m^3) and buoyancy (Brunt-Väisälä) frequency (cycl/h) at station 17802 (WOD13) located in Fig. 1. The yellow stripes indicate areas potentially correlated with internal wave generation at interfaces between Subtropical Surface Water (STSW) and South Indian Central Water (SICW), and between SICW and Antarctic Intermediate Water (AAIW). (For interpretation of the references to colour in this figure legend, the reader is referred to the Web version of this article.)

(Fig. 8) cover T1, T2, T3 and T4. These show that terraces occur close to the present water depth range of various water mass interfaces. For example, terrace T1 with Tropical + Subtropical Surface Water (TSW + STSW)/South Indian Central Water (SICW) interface, terrace T2 with SICW/Antarctic Intermediate Water (AAIW) interface, and terraces T3 and T4 with AAIW/North Atlantic Deep Water (NADW) interface. The interfaces (pycnoclines) for T1 and T2 represent sharp and well-defined density gradients (Fig. 9C). A 700 m thick transition zone marks the interface for T3 and T4 between AAIW (800–1500 m wd) and NADW (2200–3500 m wd). The transition zone is marked by a diffuse density gradient with a gradual transition from one water mass to the other (Fig. 9C). These interfaces can be affected by different oceanographic processes, which are described below.

5.1.1. *The effect of internal tides*

According to both in situ measurements (tidal gauges) and numerical models, the most important harmonic affecting the Mozambique Channel is semi-diurnal (M_2 tidal constituent; 12.42 h) tides (sea-level amplitudes up to 2 m) (Chevane et al., 2016). Manders et al. (2004) demonstrated that the barotropic tidal current (with the dominant M_2 component) velocity oscillates within ± 2–5 cm/s in north-south direction. The east-west oriented tidal current oscillates within ± 1 cm/s and is thus negligible, except along the shelf (30–70 cm/s; Chevane et al., 2016). Interaction between the barotropic tidal current with the bottom topography, in regions where it changes more or less abruptly, as ridges, banks, slopes, shelf breaks, etc., may often result in the generation of large internal waves of tidal period, known as internal (baroclinic) tides (Shanmugam, 2013; Hernández-Molina et al., 2016b). According to Manders et al. (2004), internal semi-diurnal tidal current oscillates within ± 3–4 cm/s, with peaks exceeded 12 cm/s (~250 m wd). Internal waves of tidal period (M_2) are also a major driving force for vertical displacements of the isopycnals (Maas et al., 2018). Isopycnal displacement (~100 m) produced by internal waves propagation can be observed directly from Envisat advanced synthetic aperture radar (ASAR) images (Fig. 10). It shows clear evidence of internal waves travelling oceanward away from the shelf break (Fig. 10E and 10D) and toward the continental shelf (Fig. 10A, B, and 10C). In Fig. 9, higher buoyancy (Brunt-Väisälä) frequency is observed on the proximal and/or nearly flat sector of terrace T1. It coincides with the water depth range of the interface between TSW + STSW/SICW (~200 m wd). Da Silva et al. (2009) observed internal waves travelling at 1.4 m/s with wavelengths of 0.5 km along the pycnocline near the surface (~60–100 m). It leads to oscillation around 10 cycl/h which is consistent with values observed along T1 at ~100 m wd (Fig. 9B). For T2, high values of buoyancy (Brunt-Väisälä) frequency along the water depth range of the interface between SICW/AAIW (~800 m wd) (Fig. 9A) indicate a stably-stratified boundary layer, allowing for internal waves to propagate (Maas et al., 2018). Lastly, Maas et al. (2018) indicated that the fluctuation of the isopycnal (displacements of 80 m) at 1500 wd was in general dominated by the internal tides, as reported for internal waves above. This fact point to a probable propagation of internal waves in the water depth range of T3. However, the study of

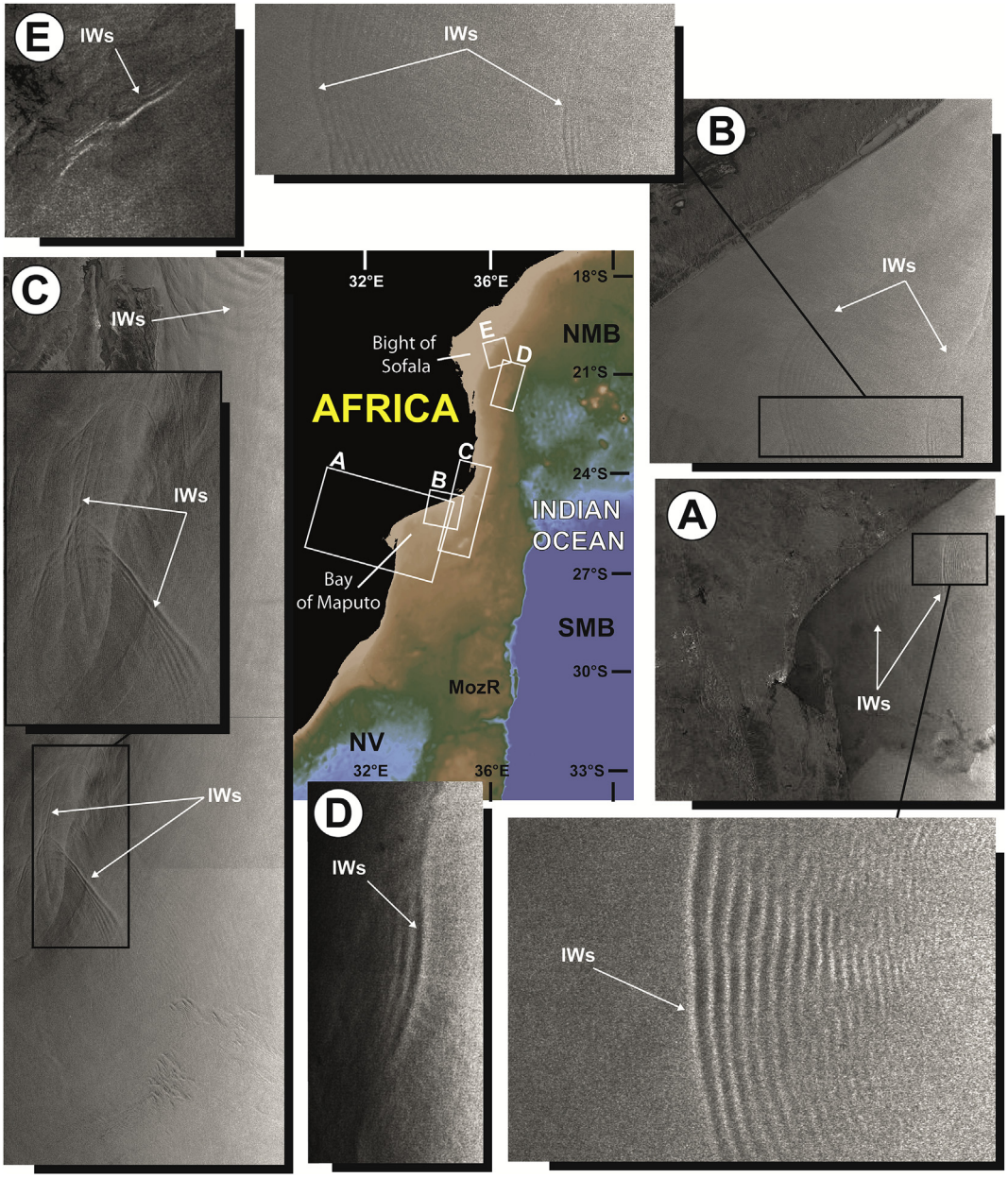

Fig. 10. Select examples of internal waves (solitons) propagating along the Mozambique Channel. Images (A–C) are located along the Bay of Maputo (from Jackson, 2004) and (D–E) are along the Bight of Sofala (from Magalhaes et al., 2014). Abbreviations: NMB = Northern Mozambique Basin; SMB = Southern Mozambique Basin; NV = Natal Valley; MozR = Mozambique Ridge; IWs = Internal waves.

Maas et al. (2018) is located along the narrowest part of the Mozambique Channel (17° S) while T3 occurs at around 22° S (Fig. 4). This assumption remains nevertheless to be confirmed by further studies. Hence, we suggest that internal waves of tidal period may act as the primary mechanism in the erosion or non-deposition of contourite terraces T1, T2 and T3 as have been proposed along the south Atlantic continental slopes (e.g., Hernández-Molina et al., 2009; Preu et al., 2013). These can mobilize and re-suspend bottom sediments (e.g., Cacchione et al., 2002; McCave, 2009; Pomar et al., 2012; Shanmugam, 2013).

5.1.2. The effect of eddies

Mesoscale eddies (either cyclonic or anticyclonic) can be considered as a further mechanism (e.g., García et al., 2015). Such eddies are well described along the Mozambique Channel (De Ruijter et al., 2002). These eddies have a large barotropic component, affecting the whole water column with current velocities ~50 - 25 cm/s at ~200–300 m wd, respectively (Ternon et al., 2014). Current velocities are, however, greatly weakened near the bottom (~10 cm/s at depths > 2000 m) (Schouten et al., 2003). Consequently, these eddies were able to induce erosion or non-deposition along the contourite terraces. This finding is consistent with the area of erosion or non-deposition of T1 along the Inharrime Terrace (Martin, 1981) (Fig. 4) maintained by strong bottom currents due to eddies (Lamont et al., 2010; Preu et al., 2011). As a final remark, internal waves are also likely to be amplified by interaction with mesoscale eddies (Magalhaes et al., 2014; Xie et al., 2015). Beal et al. (2006) also suggested eddy-induced generation of internal waves along the upper boundary of the NADW (~2200 m wd) in the water depth range of T4 (e.g., Clément et al., 2017).

5.1.3. The effect of along-slope bottom currents

Another possible mechanism controlling sediment dynamics

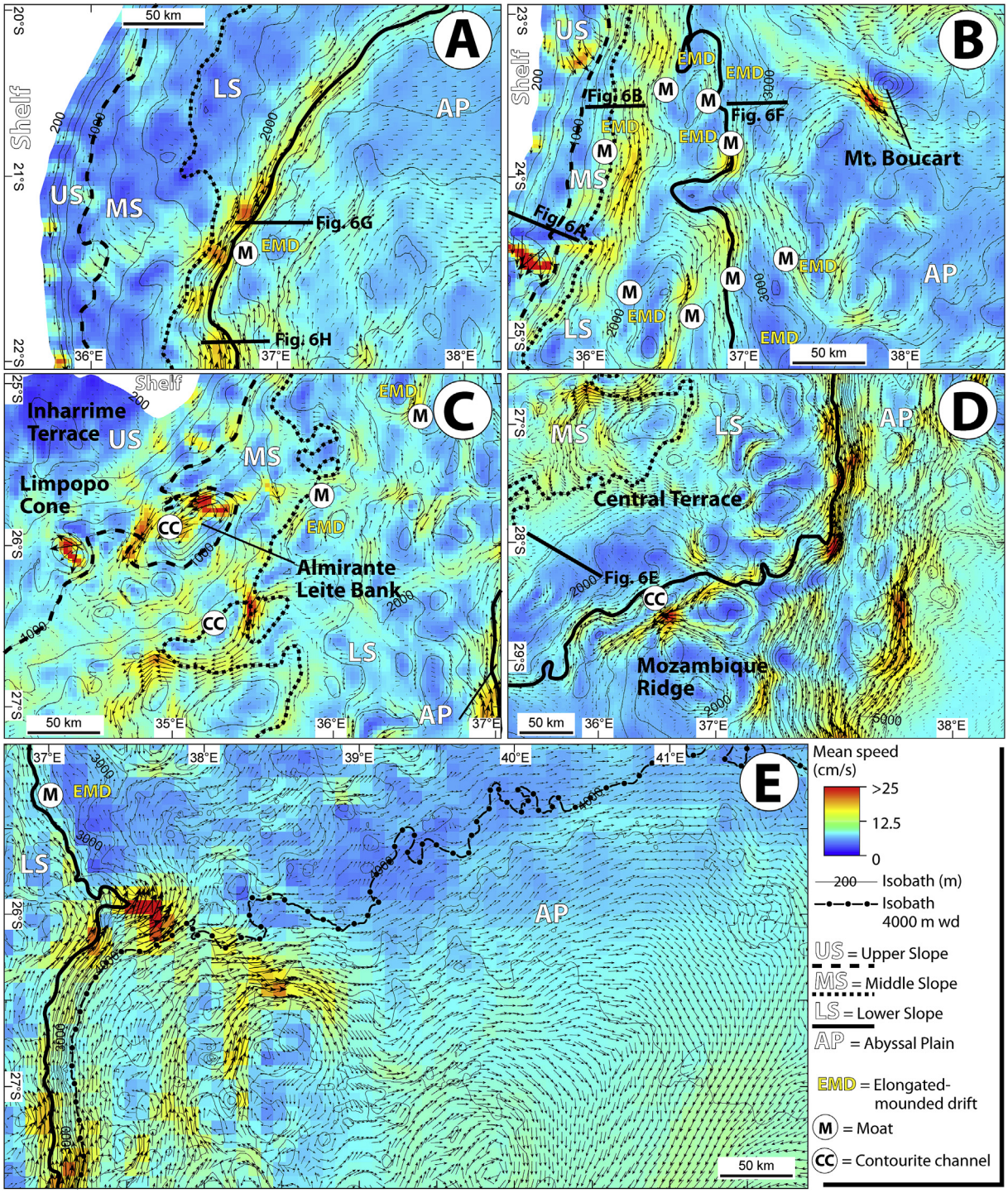

Fig. 11. Results from the Regional Oceanic Modelling System (ROMS) showing mean bottom current velocities along the seafloor of five different sectors indicated in Fig. 4.

originates from the along-slope bottom currents. Fig. 11 shows clear evidence for high current velocities influencing T3 and T4 (> 25 cm/s). For T3, Beal (2009) reported northward flow velocities of 25 cm/s with peak speed over 95 cm/s at ~1400 m wd within the Agulhas undercurrent (1000–2900 m wd). Ridderinkhof and de Ruijter (2003) interpreted northward flow velocities of 4.5 cm/s with peak speed around 40 cm/s at 1500–2400 m wd within the Mozambique undercurrent. However, it should be noted that geostrophic flows have periods of intense, reduce or even revert circulation modulated by periodic or a-periodic processes (eddies, deep water tidal currents, etc.). Additionally, internal waves may be generated when the along-slope bottom currents flow over rough topography (Liang and Thurnherr, 2012).

5.2. Along-slope bottom current circulation governs the formation of plastered drifts

Large-scale plastered drifts (D1 and D2) occur on a regional scale along the Mozambican margin while plastered drift D3 occurs on a more local scale (Fig. 4). These occur in basinward areas and in distal

areas of contourite terraces T1, T2 and T3, respectively (Fig. 6A, C, and 6E). Plastered drift water depths range from ~300–600 m for D1, ~900–1300 m for D2 and ~1600 to ~2200 m for D3. Their distribution determines morphological seafloor changes that roughly coincide with the major physiographic provinces (D1, upper slope; D2, middle slope; and D3, lower slope; Fig. 5 and 6). Thus, these have significant effect in the shaping of the continental margin (e.g., Mosher et al., 2017). Hydrographic sections indicate that D1 and D2 match the near-bottom layer distribution of water masses bounded by the most pronounced density contrasts (pycnoclines) (Fig. 9). We therefore interpret large plastered drifts D1 and D2 along the Mozambican slope as influenced by the SICW (200–600 m wd) and AAIW (800–1500 m wd), respectively (Fig. 8A and 8B). In contrast, plastered drift D3 occurs in the transition zone between AAIW (800–1500 m wd) and NADW (2200–3500 m wd). Along-slope bottom currents move relatively slowly in the water depth range occupied by the plastered drifts (~5–10 cm/s) (Fig. 11). These currents exhibit generally southward direction over D1 (Fig. 11A), and northward direction over D2 and D3 (Fig. 11B and 11D). This hypothesis is further confirmed by other studies: Martin (1981) demonstrated that rapid sediment accumulation of D1 along the Inharrime Terrace occurs under weak southward flow conditions; and Beal (2009) reported weak northward flow velocities of 10 cm/s at 1100 m wd in the water depth range of D2.

These morpho-sedimentary and hydrographic coincidences lead us to propose that the regional physiographic configuration of the Mozambican margin is most likely related to along-slope bottom currents. Seismic profiles indicate that the present-day physiographic configuration and the sub-bottom architecture of the plastered drifts have a stable behaviour on geological timescales, as reported by Dingle et al. (1978) and Preu et al. (2011) for D1 along the Inharrime Terrace. It allows us to suggest a long-term, stable behaviour of the water masses (e.g., Rebesco et al., 2014; Ercilla et al., 2016). Thus, the observed variability of geostrophic flows in the region (eddies, deep water tidal currents, etc.) appears to have no significant effect in the long-term shaping of the continental margin. Although their apparent not significant effect may simply reflect poor interpretation because their importance cannot be resolved in our seismic profiles. This point was mentioned in the study of Ercilla et al. (2016). Lastly, the actual oceanographic model and all observed variability (eddies, deep water tidal currents, etc.) might differ over the geological time span of plastered drifts formation. This scenario might explain the present-day unusual location of D3 in the water depth range of the transition zone between two water masses (AAIW and NADW).

5.3. Influence of bottom topography on bottom current processes

The AAIW and NADW encounter obstacles such as seamounts (i.e., Almirante Leite Bank, Naudé Ridge), the Beira High and the Mozambique Ridge. These obstacles produce streamline distortions, creating current cores that can winnow, distribute, erode, and rework near-surface sediment (e.g., Kennett, 1982; Faugères et al., 1999; García et al., 2009). The AAIW and NADW usually have main current cores that run northward, parallel to isobaths along the walls of the obstacles (e.g., Dingle et al., 1987) (Fig. 11). The velocity of these cores manifests in erosive features (moats, contourite channels, abraded surfaces, and lineations; scours and furrows) (Fig. 4). Moats are associated with elongated-mounded drifts at the foot of high walls, as well as the abraded surfaces along their walls (e.g., Kennett, 1982; Hernández-Molina et al., 2006b) (Figs. 4–6). These features suggest helicoidal flows around the cores of the current, referred to as 'horizontal eddies' (Rebesco et al., 2014). It result from Coriolis effect directing the cores of the current against the adjacent slope eroding the left side of the moat and depositing sediment on the right side where the current velocity is lower (e.g., Llave et al., 2001; Faugères and Mulder, 2011). The currents then form the abraded surfaces north of the Naudé Ridge (Fig. 6D) and along the steep lower-slopes of the Mozambique margin (Figs. 5B, 6G and 6H). They also influence contourite channels and moats along the Almirante Leite Bank (Fig. 4), on the Mozambican lower-slope (Fig. 5B and 6B), at the foot of the Mozambique Ridge (Figs. 5B, 6F and 6G), and eastern-limb of the Beira High (Fig. 6G), and across deep, E-W corridors within the Mozambique Ridge (Fig. 4; described in Wiles et al., 2014). Finally, they form elongated-mounded drifts immediately seaward of moats (Figs. 5B, 6B and 6F, and 6G). As shown in Fig. 11, bands of high bottom current velocities (> 25 cm/s) correspond either to the presence of moats/contourite channels or abraded surfaces, while elongated-mounded drifts experience the lowest bottom current velocities (< 12.5 cm/s). Both are associated with northward flowing water masses of the AAIW and NADW within the Mozambique and Agulhas undercurrents. However, Fig. 11C shows the complexity of AAIW circulation, a large part of which is diverted southward. Observations of Dingle et al. (1978) and Martin (1981) support the interpretation given here by emphasizing that the deepest moats lie along upstream (NE) flanks of topographic highs centered on the Almirante Leite Bank between ~900 and 1300 m wd. This suggests southward flow of the AAIW following the model of Faugères et al. (1999), Llave et al. (2001), and Hernández-Molina et al. (2006b). Re-circulation of the AAIW may be due to the occurrence of passing moving anticyclonic eddies that also carry the RSW southward at a depth of ~900–1200 m (Gründlingh, 1985; Ridderinkhof and de Ruijter, 2003). Beal (2009) also defined the core of the Agulhas undercurrent at 1000–2900 m wd, where it carries both AAIW and NADW northward. For the northern part of the Mozambique Channel near 17° S, Ridderinkhof and de Ruijter (2003) interpreted the core of the Mozambique undercurrent at 1500–2400 m wd and suggested entrainment of the AAIW southward where it exits the local undercurrent.

Sedimentary waves at water depths of 2500–3500 m along the abyssal plain are linked to the presence of the NADW, which would be locally guided by seafloor irregularities and incisions created by the Zambezi Valley and seamounts (i.e., Bassas Da India, Mt. Boucart) (Fig. 4 and 11). Breitzke et al. (2017) demonstrated that these sedimentary waves are draped with sediments, indicating that present-day velocities cannot erode sediments along this part of the abyssal plain. At water depths greater than ~3500 m, Breitzke et al. (2017) described bedforms as consisting mainly of large sedimentary waves, giant erosional scours, and furrows. These occur in the transition zone (~500 m) between the NADW (< 3500 m) and the AABW (> 4000 m) and within the AABW. Crests tend to be aligned oblique to the current direction in the case of sedimentary waves associated with geostrophic bottom currents (Fox et al., 1968; Manley and Flood, 1993). Simulation results (Fig. 11E) demonstrate that bottom currents direction is consistent with the oblique alignments of the sediment wave crests (Fig. 4). Here, the shallow bathymetry (< 4000 m wd) of the northern part of the margin topographically blocks the AABW to the north and deflects it eastward. Thus, we can infer that these features likely result from the geostrophic flows (~12.5 cm/s), being aided by internal waves in the transition zone of NADW and AABW (3500–4000 m wd) (Kolla et al., 1980). Furrows, observed to run oblique relative to the main bottom currents, and scours point toward the northward flowing AABW (Fig. 4 and 11E). Furthermore, high northward flow velocities (> 25 cm/s) at the foot of the Mozambique Ridge (along 37° E, Fig. 11E) suggest the role of 'horizontal eddies' in generating these features (e.g., Hernández-Molina et al., 2014).

5.4. A model for deep-sea sedimentation in the Mozambique channel

We present a new model for deep-sea sedimentation within the Mozambique Channel (Fig. 12). Sediments from the continent are mainly transported by the Zambezi, Limpopo, and Tugela rivers. When these rivers reach coastal areas, the Mozambique Current and Agulhas Current quickly disperse the suspended sediment over large areas along the continental shelf and upper slope. The Mozambique Undercurrent and Agulhas Undercurrent subsequently transport and deposit the

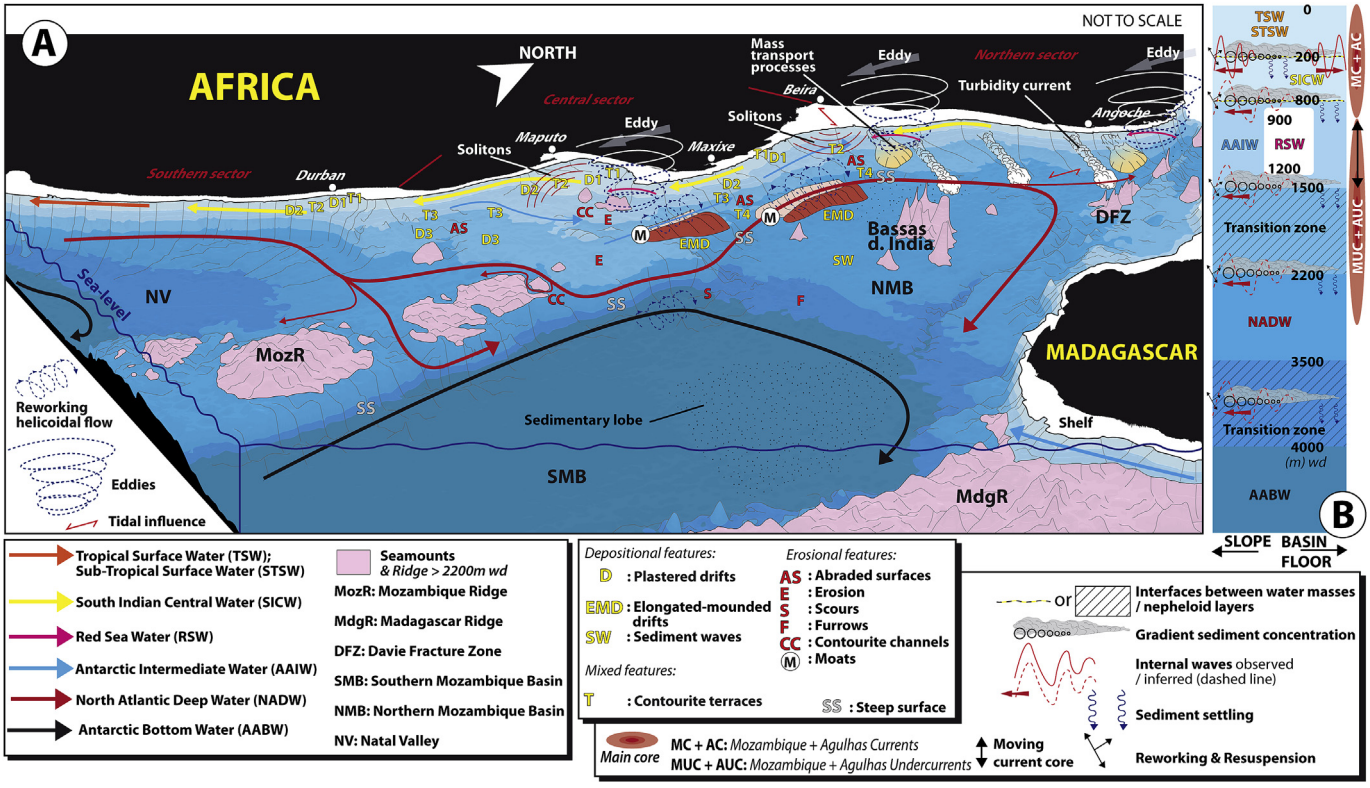

Fig. 12. (A) 3D sketch summarizing the conceptual model of the effect of bottom current processes on deep-water sedimentation along the Mozambique Channel. Simplified morpho-sedimentary and hydrographic features are shown. (B) Schematic model for the Mozambique Channel explaining water mass interface processes.

sediment along the middle-lower slopes, base-of-slope, seamount flanks, and abyssal plain. The TSW + STSW (+Tropical Thermocline Water)/SICW, SICW/AAIW (+RSW), AAIW (+RSW)/NADW, and NADW/AABW interfaces along the Mozambican margin form superimposed nepheloid layers by settling processes (McCave and Tucholke, 1986; Preu et al., 2013). For example, fine-grained sediments arriving as turbidity currents from the continent are remobilized by the NADW/AABW interface and subsequently concentrated into a dense nepheloid layer between 3500 and 4500 m wd (Kolla et al., 1980). These layers represent a major regional/basin scale transport mechanism for fine-grained sediments at different water depths. They deposit sediments laterally and basinward with a dominant along-slope component. Material in the Mozambique Channel can thus experience significant transport over long distances prior to deposition. Turbulent processes generated at the interfaces (e.g., internal waves) interacting with the continental slope/shelf may induce bottom current erosion, re-suspension, and redistribution of sediment (e.g., Dickson and McCave, 1986; Cacchione et al., 2002; Pomar et al., 2012; Shanmugam, 2013, 2014). These mechanisms change slope morphology by steepening upslope and developing a terrace-like feature along the water mass interface (Hernández-Molina et al., 2009; Preu et al., 2013). This sweep and winnow of the seafloor may also supply the nepheloid layers with sediment at the seaward limit of the terrace (Dickson and McCave, 1986; Puig et al., 2004; Wilson et al., 2015). Kolla et al. (1980) suggested that sedimentary waves on the Mozambican abyssal plain can result from very deep internal waves (e.g., van Haren and Gostiaux, 2011) focused on the nepheloid layer at the NADW/AABW interface between 3500 and 4500 m wd. Deposition occurs mainly in areas experiencing relatively low current velocities where settling of suspended particles can form contourite drifts (Miramontes et al., 2016; Cattaneo et al., 2017). Large-scale velocity variation in current pathways may reflect strong rotational current velocities (> 70 cm/s) due to southward moving anticyclonic eddies (Ridderinkhof and de Ruijter, 2003) interacting with the Mozambican margin morphology (Dingle et al., 1987). Contourite drifts can also form from local reworking of the seafloor by bottom currents (e.g., 'horizontal eddies'). In this case, topography influences the velocity of the impinging water-mass and sediments deposit near the eroded source area (Rebesco and Camerlenghi, 2008). Coriolis forcing of northward currents towards the Mozambican margin (e.g., Faugères and Mulder, 2011) can amplify this effect. In the depositional model for the Mozambique Channel described here, most present-day sedimentary processes and their morpho-sedimentary products result from bottom current processes. Observations from similar European and South American margins (Hernández-Molina et al., 2011, 2016a; Ercilla et al., 2016; Preu et al., 2013) support this interpretation.

Based on our results, two important aspects should be considered for improving this sedimentary model in the future. First, we show a dominance of across-slope gravity-driven processes operating along the northern sector of the Mozambican margin (Fig. 4). Slope and shelf areas associated with the northern sector experienced high rates of sediment than those located in the central and southern sectors (e.g., estimated present annual sedimentary input: $100{\cdot}10^6$ t from the Zambezi River; $4.8{\cdot}10^6$ t from the Limpopo River, Milliman, 1981). In the northern sector, high rates of sediment delivery beginning in the Pliocene and continuing up to present (Dingle et al., 1983; Walford et al., 2005; Franke et al., 2015) may have conditioned large MTDs and maintained turbidity currents through time. In the central and southern sectors, limited sediment supply between the Pliocene and present (Green et al., 2008; Green, 2011; Said et al., 2015; Hicks and Green, 2016) led to a predominance of along-slope (contourite) processes. The northern sector, however reveals a combination of along-slope (i.e., T1 and D1) and across-slope (i.e., MTDs, turbidity currents) processes that may be related to sea-level fluctuations during glacial and inter-glacial periods (Wiles et al., 2017). During interglacial periods, sediments in front of the Zambezi River (*'inner mud belt'*) are transported northward along the *'inner'* shelf. Much of these sediments transfer through upper slope canyons of the Angoche SCS, few of these sediments are transported southward along the *'outer'* shelf (*'outer mud belt'*) toward the

Middle and Lower Zambezi SCSs (Schulz et al., 2011; Wiles et al., 2017) (Fig. 4). This flux can be expected to have resulted in greater downslope transport (i.e., MTDs and turbidity currents) in front of the Angoche SCS than in front of the Middle and Lower Zambezi SCSs as it reached the shelf edge (Wiles et al., 2017) and may inhibit along-slope processes and their sedimentary features. Furthermore, shelf morphology (depth of the shelf-break, width of the shelf, etc.) during interglacial periods (such as in present-day, Wiles et al., 2017) is suitable for internal waves to propagate along the shelf edge, especially in front of the Middle and Lower Zambezi SCSs (Da Silva et al., 2009). Internal waves contributed to erosion, re-suspension, and redistribution of sediments along the upper slope, forming contourite terrace T1 and plastered drift D1 (e.g., Preu et al., 2013). During glacial periods, greater sediments supply and variation of the shelf morphology in front of the Middle and Lower Zambezi SCSs probably facilitate downslope sediment transport (Wiles et al., 2017) along the continental slope as well as preclude generation of internal waves. Further research can confirm or refute this hypothesis.

Second, a particular deep plastered drift (D3) occurs over a specific water depth range in the transition zone between two water masses (AAIW and NADW) while upper plastered drifts (D2 and D3) match water depth ranges of water masses (SICW and AAIW) between density interfaces (pycnoclines) (e.g., Preu et al., 2013; Rebesco et al., 2014). However, the interpretation of D3 being generated in the transition zone between two water masses is questionable and it could be related to vertical movement of interfaces. The plastered drift formation is the result of processes acting on longer geological times. During the Quaternary, the Atlantic and Southwest Indian water-mass circulation and spatial fluctuations in water-mass interfaces may have been controlled by the Agulhas leakage (Hall et al., 2017) with less leakage during full glacial times than interglacial times (Peeters et al., 2004; Caley et al., 2012; Petrick et al., 2015). Variations of the Agulhas leakage have led to a weakening of the NADW flow during glacial stages, allowing the deep Antarctic water masses (CDW and AABW) to extend farther north than it does today (Bickert and Wefer, 1996; Pena and Goldstein, 2014). During cold (glacial) periods under this scenario, the oceanographic setting would differ from the present one and may have potentially provoked vertical and lateral variations of the interfaces and the associated oceanographic processes (e.g., internal waves), displacing drift D3 under the influence of deep Antarctic water masses. This interpretation is supported by Breitzke et al. (2017) suggesting that sedimentary waves under the water depth range of the NADW along the abyssal plain (Fig. 4) are draped with sediments. Thus, sedimentary waves might be related to strong bottom currents during cold periods, potentially under the AABW flow. While the discussion given above is somewhat speculative, and open a discussion proposed by Preu et al. (2013) in Argentine/Uruguay and Hernández-Molina et al. (2017b) in the Pacific margin of the Antarctic Peninsula about if some deep water features in the ocean are functional or relict. Are observed drifts and contourite terraces identify in deep-environments (lower slope and basin floor) relate to the same water masses structure than observed today? The conditions and timing of their formation, remain still unresolved but future research should address these questions.

6. Conclusion

This work interpreted a number of large contourite deposits along the Mozambique Channel and their associated bottom currents and oceanographic processes. The oceanographic processes described act in combination to determine the bottom current's local direction and velocity. Although many of these processes and their effects on deep-water sedimentation are not fully understood, local or regional interaction of these processes with the seafloor influences morphology and sediment distribution along the Mozambican continental margin and adjacent Durban basin. This study came to fourth major conclusions:

a) The first and most important finding is that internal waves originate from instabilities in the transition zone (interfaces/pycnoclines) between two water masses, caused by eddies, tidal and geostrophic currents being aided by topography. It provides the most plausible mechanism for sculpting contourite terraces (T1 to T4 in this study), facilitating erosion, re-suspension and redistribution of sediments (e.g., nepheloid layers).
b) Second, weak along-slope bottom currents on the plastered drifts (D1 to D3) rarely exceed 12.5 cm/s and thus promote the settling of suspended particles. Growth of plastered drifts D1 and D2 is facilitated by weak along-slope bottom currents of two major water-masses circulating in the Mozambique Channel (i.e., SICW and AAIW) or a counteraction of such currents with periodic or a-periodic processes (e.g., eddies, deep water tidal currents), reducing current velocities.
c) Third, the strengthening of along-slope bottom currents (e.g., Coriolis Effect, eddies, deep water tidal currents), being aided by seafloor irregularities would result in 'horizontal eddies'. Hence, these currents lead to erosion inside the moat and deposition on the elongated-mounded drift. Our study show that these drifts can develop inside the transition zone. Nevertheless, the finding in our study and limitations in the hydrodynamic modelling (e.g., secondary processes) point out a need for further studies, not only based on numerical simulations but also by field measurements (i.e., sedimentary cores and mooring scheme) to better quantify the impact of instabilities on contouritic depositional systems.
d) The fourth finding is that the specific plastered drift D3 in our study area occurs in the transition zone between two water masses (AAIW and NADW), and forms on a much smaller lateral scale. This marks a major difference between the plastered drift investigated here and the existing paradigm that plastered drifts are often formed below water mass interfaces (such as D1 and D2). A possible explanation for that could be related to the fact that, through geological times, vertical movements of water masses and associated interfaces occurred, as reported in the south Atlantic by Preu et al. (2013), where the AABW was thicker, more vigorous and its top quite shallower during glacial stages compared with interglacial stages, as the present one. This hypothesis highlight new and important considerations: are all present morphologies in deep marine environment functional? Can some depositional and erosional features, especially in the deepest oceans, be relicts, being active under different oceanographic processes than the present ones?

Acknowledgments

The Authors sincerely thank TOTAL S.A., WesternGeco, and CGG for permission in using seismic datasets. We also thank to the reviewers for their suggestions that helped us to improve the paper. The research formed part of Ph.D. thesis for A. Thiéblemont funded by TOTAL as part of the Frontier Exploration research program. Elda Miramontes' Post-Doctoral fellowship was co-funded by TOTAL and IFREMER as part of the PAMELA (Passive Margin Exploration Laboratory) scientific project. The research was conducted in the framework of 'The Drifters Research Group' of the Royal Holloway University of London (UK), and it is related to the projects CTM 2012-39599-C03, CGL2016-80445-R and CTM2016-75129-C3-1-R.

References

Coffin, M.F., Rabinowitz, P.D., 1992. The Mesozoic East African and Madagascan conjugate continental margins; stratigraphy and tectonics. In: Watkins, J.S., Zhigiang, F., McMillen, K.J. (Eds.), Geology and Geophysics of Continental Margins. vol. 53. AAPG, pp. 207–240. https://doi.org/10.1306/M53552C12.

Amante, C., Eakins, B.W., 2009. ETOPO1 1 Arc-Minute Global Relief Model: Procedures, Data Sources and Analysis. NOAA Technical Memorandum NESDIS NGDC-24. National Geophysical Data Center, NOAA. https://doi.org/10.7289/V5C8276M.

Beal, L.M., 2009. A time series of Agulhas undercurrent transport. J. Phys. Oceanogr. 39,

2436–2450. https://doi.org/10.1175/2009JPO4195.1.
Beal, L.M., Ffield, A., Gordon, A.L., 2000. The spreading of Red Sea overflow waters in the Indian Ocean. J. Geophys. Res. Ocean. 105 (C4), 8549–8564. https://doi.org/10.1029/1999JC900306.
Beal, L.M., Chereskin, T.K., Lenn, Y.D., Elipot, S., 2006. The sources and mixing characteristics of the Agulhas Current. J. Phys. Oceanogr. 36 (11), 2060–2074. https://doi.org/10.1175/JPO2964.1.
Bickert, T., Wefer, G., 1996. Late quaternary deep water circulation in the South Atlantic: Reconstruction from carbonate dissolution and benthic stable isotopes. In: Wefer, G., Berger, W.H., Siedler, G., Webb, D.J. (Eds.), The South Atlantic: Present and Past Circulation. Springer-Verlag Berlin Heidelberg, pp. 599–620. https://doi.org/10.1007/978-3-642-80353-6_30.
Breitzke, M., Wiles, E., Krocker, R., Watkeys, M.K., Jokat, W., 2017. Seafloor morphology in the Mozambique Channel: evidence for long-term persistent bottom-current flow and deep-reaching eddy activity. Mar. Geophys. Res. 38 (3), 241–269. https://doi.org/10.1007/s11001-017-9322-7.
Broad, D.S., Jungslager, I.R., McLachlan, I.R., Roux, J., 2006. Offshore mesozoic basins. In: Johnson, M.R., Abhaeusser, C.R., Thomas, R.J. (Eds.), The Geology of South Africa. Geological Society of South Africa/Council for Geoscience, Johannesburg/Pretoria, pp. 553–571.
Cacchione, D.A., Pratson, L.F., Ogston, A.S., 2002. The shaping of continental slopes by internal tides. Science 296, 724–727. https://doi.org/10.1126/science. 1069803.
Caley, T., Giraudeau, J., Malaizé, B., Rossignol, L., Pierre, C., 2012. Agulhas leakage as a key process in the modes of Quaternary climate changes. Proc. Natl. Acad. Sci. U.S.A. 109 (18), 6835–6839. https://doi.org/10.1073/pnas.1115545109.
Castelino, J., Reichert, C., Klingelhoefer, F., Aslanian, D., Jokat, W., 2015. Mesozoic and Early Cenozoic sediment influx and geomorphology of the Mozambique Basin. Mar. Petrol. Geol. 66, 890–905. https://doi.org/10.1016/j.marpetgeo.2015.07.028.
Cattaneo, A., Miramontes, E., Samalens, K., Garreau, P., Caillaud, M., Marsset, B., Corradi, N., Migeon, S., 2017. Contourite identification along Italian margins: The case of the Portofino drift (Ligurian Sea). Mar. Petrol. Geol. 87, 137–147. https://doi.org/10.1016/j-marpetgeo.2017.03.026.
Chevane, C., Penven, P., Nehama, F., Reason, C., 2016. Modelling the tides and their impacts on the vertical stratification over the Sofala Bank, Mozambique. Afr. J. Mar. Sci. 38 (4), 465–479. https://doi.org/10.2989/1814232X.2016.1236039.
Clément, L., Frajka-Williams, E., Sheen, K.L., Brearley, J.A., Naveira Garabato, A.C., 2017. Generation of internal waves by eddies impinging on the western boundary of the North Atlantic. J. Phys. Oceanogr. 46, 1067–1079. https://doi.org/10.1175/JPO-D-14-0241.1.
Coffin, M.F., Rabinowitz, P.D., 1987. Reconstruction of Madagascar and Africa: Evidence from the Davie fracture zone and western Somali basin. J. Geophys. Res. 92 (B9), 9385–9406. https://doi.org/10.1029/JB092iB09p09385.
Courgeon, S., Jorry, S.J., Camoin, G.F., BouDagher-Fadel, M.K., Jouet, G., Révillon, S., Bachèlery, P., Pelleter, E., Borgomano, J., Poli, E., Droxler, A.W., 2016. Growth and demise of Cenozoic isolated carbonate platforms: New insights from the Mozambique Channel seamounts (SW Indian Ocean). Mar. Geol. 380, 90–105. https://doi.org/10.1016/j.margeo.2016.07.006.
Creaser, A., Hernández-Molina, F.J., Badalini, G., Thompson, P., Walker, R., Soto, M., Conti, B., 2017. A Late Cretaceous mixed (turbidite-contourite) system along the Uruguayan Margin: Sedimentary and palaeoceanographic implications. Mar. Geol. 390, 234–253. https://doi.org/10.1016/j.margeo.2017.07.004.
Da Silva, J.C.B., New, A.L., Magalhaes, J.M., 2009. Internal solitary waves in the Mozambique channel: Observations and interpretation. J. Geophys. Res. Ocean. 114, C5. https://doi.org/10.1029/2008JC005125.
Davison, I., Steel, I., 2017. Geology and hydrocarbon potential of the East African continental margin: a review. Petrol. Geosci. 24, 1. https://doi.org/10.1144/petgeo2017-028.
De Ruijter, W.P.M., Ridderinkhof, H., Lutjeharms, J.R.E., Schouten, M.W., Veth, C., 2002. Observations of the flow in the Mozambique channel. Geophys. Res. Lett. 29 (10), 140–141. 140-3. https://doi.org/10.1029/2001GL013714.
Debreu, L., Marchesiello, P., Penven, P., Cambon, G., 2012. Two-way nesting in split-explicit ocean models: algorithms, implementation and validation. Ocean Model. 49-50, 1–21. https://doi.org/10.1016/j.ocemod.2012.03.003.
Dee, D., Uppala, S., Simmons, A., Berrisford, P., Poli, P., Kobayashi, S., Vitart, F., 2011. The ERA-Interim reanalysis: Configuration and performance of the data assimilation system. Q. J. R. Meteorol. Soc. 137, 553–597. https://doi.org/10.1002/qj.828.
Dickson, R., McCave, I.N., 1986. Nepheloid layers on the continental slope west of Porcupine Bank. Deep Sea Res. Part A. Oceanogr. Res. Pap. 33 (6), 791–818. https://doi.org/10.1016/0198-0149(86)90089-0.
DiMarco, S.F., Chapman, P., Nowlin Jr., W.D., Hacker, P., Donohue, K., Luther, M., Johnson, G.C., Toole, J., 2002. Volume transport and property distributions of the Mozambique channel. Deep-Sea Res. Part II Top. Stud. Oceanogr. 49 (7–8), 1481–1511. https://doi.org/10.1016/S0967-0645(01)00159-X.
Dingle, R.V., Goodlad, S.W., Martin, A.K., 1978. Bathymetry and stratigraphy of the northern Natal Valley (SW Indian Ocean): a preliminary account. Mar. Geol. 20, 89–106. https://doi.org/10.1016/0025-3227(78)90099-3.
Dingle, R.V., Siesser, W.G., Newton, A.R., 1983. Mesozoic and Tertiary Geology of Southern Africa: A Global Approach to Geology. vol. 375 A.A.Balkema, Rotterdam 9789061910992.
Dingle, R.V., Birch, G.F., Bremner, J.M., De Decker, R.H., Du Plessis, A., Engelbrecht, J.C., Fincham, M.J., Fitton, T., Flemming, B.W., Goodlad, S.W., Gentle, R.I., Martin, A.K., Mills, E.G., Moir, G.J., Parker, R.J., Robson, S.H., Rogers, J., Salmon, D.A., Siesser, W.G., Simpson, E.S.W., Summerhayes, C.P., Westall, F., Winter, A., Woodborne, M.W., 1987. Deep-sea sedimentary environments around southern Africa (SE-Atlantic & SW-Indian Oceans). Ann. S. Afr. Mus. 98, 1–27.
Donohue, K.A., Beal, L.M., Firing, E., 2000. Comparison of three velocity sections of the Agulhas current and Agulhas undercurrent. J. Geophys. Res. 105 (C12), 28585–28593. https://doi.org/10.1029/1999JC000201.
Eagles, G., König, M., 2008. A model of plate kinematics in Gondwana breakup. Geophys. J. Int. 173 (2), 703–717. https://doi.org/10.1111/j.1365-246X.2008.03753.x.
Ercilla, G., Juan, C., Hernández-Molina, F.J., Bruno, M., Estrada, F., Alonso, B., Casas, D., Farran, M., Llave, E., García, M., Vázquez, J.T., D'Acremont, E., Gorini, C., Palomino, D., Valencia, J., El Moumni, B., Ammar, A., 2016. Significance of bottom currents in deep-sea morphodynamics: An example from the Alboran Sea. Mar. Geol. 378, 157–170. https://doi.org/10.1016/j.margeo.2015.09.007.
Fairall, C.W., Bradley, E.F., Rogers, D.P., Edson, J.B., Young, G.S., 1996. Bulk parameterization of air-sea fluxes for tropical ocean-global atmosphere coupled-ocean atmosphere response experiment. J. Geophys. Res. 101 (C2), 3747–3764. https://doi.org/10.1029/95JC03205.
Faugères, J.C., Mulder, T., 2011. Chapter 3 - Contour currents and contourite drifts. In: Hüneke, H., Mulder, T. (Eds.), Deep-Sea Sediments. vol. 63. Elsevier, pp. 149–214. https://doi.org/10.1016/B978-0-444-53000-4.00003-2.
Faugères, J.-C., Stow, D.A.V., 2008. Chapter 14 contourite drifts: Nature, Evolution and controls. In: Rebesco, M., Camerlenghi, A. (Eds.), Contourites. Developments in Sedimentology. vol. 60. Elsevier Science, Amsterdam, pp. 257–288. https://doi.org/10.1016/S0070-4571(08)10014-0.
Faugères, J.-C., Stow, D.A.V., Imbert, P., Viana, A.R., 1999. Seismic features diagnostic of contourite drifts. Mar. Geol. 162, 1–38. https://doi.org/10.1016/S0025-3227(99)00068-7.
Ferry, N., Parent, L., Garric, G., Bricaud, C., Testut, C., LeGalloudec, O., Zawadzki, L., 2012. Glorys2v1 global ocean reanalysis of the altimetric era (1992-2009) at meso-scale. Mercator Ocean-Quaterly Newsletter 44, 29–39.
Fine, R.A., 1993. Circulation of Antarctic intermediate water in the South Indian Ocean. Deep-Sea Res. Part 1: Oceanogr. Res. Pap. 40 (10), 2021–2042. https://doi.org/10.1016/0967-0637(93)90043-3.
Fischer, M.D., Uenzelmann-Neben, G., Jacques, G., Werner, R., 2017. The Mozambique Ridge: a document of massive multistage magmatism. Geophys. J. Int. 208 (1), 449–467. https://doi.org/10.1093/gji/ggw403.
Flemming, B.W., 1978. Underwater sand dunes along the southeast African continental margin-observations and implications. Mar. Geol. 26 (3–4), 177–198. https://doi.org/10.1016/0025-3227(78)90059-2.
Fox, P.J., Heezen, B.C., Harian, A.M., 1968. Abyssal antidunes. Nature 220, 470–472.
Franke, D., Jokat, W., Ladage, S., Stollhofen, H., Klimke, J., Lutz, R., Mahanjane, E.S., Ehrhardt, A., Schreckenberger, B., 2015. The offshore East African Rift System: Structural framework at the toe of a juvenile rift. Tectonics 34 (10), 2086–2104. https://doi.org/10.1002/2015TC003922.
García, M., Hernández-Molina, F.J., Llave, E., Stow, D.A.V., León, R., Fernández-Puga, M.C., Díaz del Río, V., Somoz, L., 2009. Contourite erosive features caused by the mediterranean outflow water in the Gulf of Cadiz: Quaternary tectonic and oceanographic implications. Mar. Geol. 257 (1–4), 24–40. https://doi.org/10.1016/j.margeo.2008.10.009.
García, M., Hernández-Molina, F.J., Alonso, B., Vázquez, J.T., Ercilla, G., Llave, E., Casas, D., 2015. Erosive sub-circular depression on the Guadalquivir Bank (Gulf of Cadiz): interaction between bottom current, mass wasting and tectonic processes. Mar. Geol. https://doi.org/10.1016/j.margeo.2015.10.004.
Goodlad, S.W., Martin, A.K., Hartnady, C.J.H., 1982. Mesozoic magnetic anomalies in the southern Natal Valley. Nature 295, 686–688. https://doi.org/10.1038/295686a0.
Gradstein, F.M., Ogg, J.G., Schmitz, M.D., Ogg, G.M., 2012. The Geologic Time Scale 2012. Elsevier, 9780444594488pp. 1176.
Green, A., 2011. Submarine canyons associated with alternating sediment starvation and shelf-edge wedge development: Northern KwaZulu-Natal continental margin, South Africa. Mar. Geol. 284, 114–126. https://doi.org/10.1016/j.margeo.2011.03.011.
Green, A.N., Ovechkina, M., Uken, R., 2008. Nannofossil age constraints on shelf edge wedge development: implications for continental margin dynamics, northern KwaZulu-Natal, South Africa. Cont. Shelf Res. 28, 2442–2449. https://doi.org/10.1016/j.csr.2008.06.007.
Gruetzner, J., Uenzelmann-Neben, G., 2015. Contourite drifts as indicators of Cenozoic bottom water intensity in the eastern Agulhas Ridge area, South Atlantic. Mar. Geol. 378, 350–360. https://doi.org/10.1016/j.margeo.2015.12.003.
Gründlingh, M.L., 1985. Occurrence of Red Sea water in the Southwestern Indian Ocean, 1981. J. Phys. Oceanogr. 15, 207–212. https://doi.org/10.1175/1520-0485(1985)015<0207:OORSWI>2.0.CO;2.
Hall, I.R., Hemming, S.R., LeVay, L.J., Barker, S., Berke, M.A., Brentegani, L., Caley, T., Cartagena-Sierra, A., Charles, C.D., Coenen, J.J., Crespin, J.G., Franzese, A.M., Gruetzner, J., Han, X., Hines, S.K.V., Jimenez Espejo, F.J., Just, J., Koutsodendris, A., Kubota, K., Lathika, N., Norris, R.D., Periera dos Santos, T., Robinson, R., Rolinson, J.M., Simon, M.H., Tangunan, D., van der Lubbe, J.J.L., Yamane, M., Zhang, H., 2017. Site U1478. and the Expedition 361 Scientists, South African Climates (Agulhas LGM Density Profile) In: Hall, I.R., Hemming, S.R., LeVay, L.J. (Eds.), Proceedings of the International Ocean Discovery Program. vol. 361 International Ocean Discovery Program, College Station, TX. https://doi.org/10.14379/iodp.proc.361.107.2017.
Halo, I., Backeberg, B., Penven, P., Ansorge, I., Reason, C., Ullgren, J.E., 2014. Eddy properties in the Mozambique Channel: A comparison between observations and two numerical ocean circulation models. Deep Sea Res. Part II Top. Stud. Oceanogr. 100, 38–53. https://doi.org/10.1016/j.dsr2.2013.10.015.
Hernández-Molina, F.J., Llave, E., Stow, D.A.V., García, M., Somoza, L., Vázquez, J.T., Lobo, F., Maestro, A., Díaz del Río, V., León, R., Medialdea, T., Gardner, J., 2006a. The contourite depositional system of the Gulf of Cadiz: a sedimentary model related to the bottom current activity of the Mediterranean outflow water and the continental margin characteristics. Deep Sea Res. Part II Top. Stud. Oceanogr. 53 (11–13), 1420–1463. https://doi.org/10.1016/j.dsr2.2006.04.016.
Hernández-Molina, F.J., Larter, R.D., Rebesco, M., Maldonado, A., 2006b. Miocene

reversal of bottom water flow along the Pacific Margin of the Antarctic Peninsula: Stratigraphic evidence from a contourite sedimentary tail. Mar. Geol. 228, 93–116. https://doi.org/10.1016/j.margeo.2005.12.010.

Hernández-Molina, F.J., Paterlini, M., Violante, R., Marshall, P., de Isasi, M., Somoza, L., Rebesco, M., 2009. Contourite depositional system on the Argentine slope: an exceptional record of the influence of Antarctic water masses. Geology 37 (6), 507–510. https://doi.org/10.1130/G25578A.1.

Hernández-Molina, F.J., Serra, N., Stow, D.A.V., Llave, E., Ercilla, G., Van Rooij, D., 2011. Along-slope oceanographic processes and sedimentary products around the Iberian margin. Geo Mar. Lett. 31 (5–6), 315–341. https://doi.org/10.1007/s00367-011-0242-2.

Hernández-Molina, F.J., Llave, E., Preu, B., Ercilla, G., Fontan, A., Bruno, M., Serra, N., Gomiz, J.J., Brackenridge, R.E., Sierro, F.J., Stow, D.A.V., García, M., Juan, C., Sandoval, N., Arnaiz, A., 2014. Contourite processes associated to the Mediterranean outflow water after its exit from the Gibraltar Strait: global and conceptual implications. Geology 42 (3), 227–230. https://doi.org/10.1130/G35083.1.

Hernández-Molina, F.J., Soto, M., Piola, A.R., Tomasini, J., Preu, B., Thompson, P., De Santa Ana, H., 2016a. A contourite depositional system along the Uruguayan continental margin: sedimentary, oceanographic and paleoceanographic implications. Mar. Geol. 378, 333–349. https://doi.org/10.1016/j.margeo.2015.10.008.

Hernández-Molina, F.J., Wåhlin, A., Bruno, M., Ercilla, G., Llave, E., Serra, N., Roson, G., Puig, P., Rebesco, M., Van Rooij, D., Roque, C., González-Pola, C., Sánchez, F., Gómez, M., Preu, B., Schwenk, T., Hanebuth, T.J.J., Sánchez-Leal, R.F., García Lafuente, J., Brackenridge, R.E., Juan, C., Stow, D.A.V., Sánchez-González, J.M., 2016b. Oceanographic processes and products around the Iberian margin: a new multidisciplinary approach. Special Issue: The Contourite Log-Book. Mar. Geol. 378, 127–156. https://doi.org/10.1016/j.margeo.2015.12.008.

Hernández-Molina, F.J., Campbell, S., Badalini, G., Thompson, P., Walker, R., Soto, M., Conti, B., Preu, B., Thieblemont, A., Hyslop, L., Miramontes, E., Morales, E., 2017a. Large bedforms on contourite terraces: Sedimentary and conceptual implications. Geology 46, 27–30. https://doi.org/10.1130/G39655.1.

Hernández-Molina, F.J., Larter, R.D., Maldonado, A., 2017b. Neogene to quaternary stratigraphic evolution of the Antarctic Peninsula, Pacific margin offshore of Adelaide Island: Transitions from a non-glacial, through glacially-influenced to a fully glacial state. Glob. Planet. Chang. 156, 80–111. https://doi.org/10.1016/j.gloplacha.2017.07.002.

Hicks, N., Green, A., 2016. Sedimentology and depositional architecture of a submarine delta-fan complex in the Durban Basin, South Africa. Mar. Petrol. Geol. 78, 390–404. https://doi.org/10.1016/j.marpetgeo.2016.09.032.

IHO and IOC, 1983. Standardization of Undersea Feature Names: Guidelines, Proposal Form, Terminology. International Hydrographic Bureau, Monaco, pp. 27.

Jackson, C.R., 2004. An Atlas of Internal Solitary-like Waves and Their Properties. Global Ocean Associates, Rockville, MD (prepared for Office of Naval Research). [Online-27/02/2018]. http://www.internalwaveatlas.com.

Jokat, W., Boebel, T., König, M., Meyer, U., 2003. Timing and geometry of early Gondwana breakup. J. Geophys. Res. 108 B9. https://doi.org/10.1029/2002JB001802.

Kennett, J., 1982. Marine Geology. vol. 813 Prentice Hall9780135569368.

Kolla, V., Eittreim, S., Sullivan, L., Kostecki, J.A., Burckle, L.H., 1980. Current-controlled, abyssal microtopography and sedimentation in Mozambique basin, Southwest Indian Ocean. Mar. Geol. 34 (3–4), 171–206. https://doi.org/10.1016/0025-3227(80)90071-7.

König, M., Jokat, W., 2010. Advanced insights into magmatism and volcanism of the Mozambique Ridge and Mozambique Basin in the view of new potential field data. Geophys. J. Int. 180 (1), 158–180. https://doi.org/10.1111/j.1365-246X.2009.04433.x.

Lamont, T., Roberts, M.J., Barlow, R.G., Morris, T., van den Berg, M.A., 2010. Circulation patterns in the Delagoa Bight, Mozambique, and the influence of deep Ocean eddies. Afr. J. Mar. Sci. 32 (3), 553–562. https://doi.org/10.2989/1814232X.2010.538147.

Leinweber, V.T., Jokat, W., 2012. The Jurassic history of the Africa-Antarctica Corridor - new constraints from magnetic data on the conjugate continental margins. Tectonophysics 530-531, 87–101. https://doi.org/10.1016/j.tecto.2011.11.008.

Leinweber, V.T., Klingelhoefer, F., Neben, S., Reichert, C., Aslanian, D., Matias, L., Heyde, I., Schreckenberger, B., Jokat, W., 2013. The crustal structure of the central Mozambique continental margin d Wide-angle seismic, gravity and magnetic study in the Mozambique channel, Eastern Africa. Tectonophysics 599, 170–196. https://doi.org/10.1016/j.tecto.2013.04.015.

Liang, X., Thurnherr, A.M., 2012. Eddy-modulated internal waves and mixing on a midocean ridge. J. Phys. Oceanogr. 42, 1242–1248. https://doi.org/10.1175/JPO-D-11-0126.1.

Llave, E., Hernández-Molina, F.J., Somoza, L., Díaz del Río, V., Stow, D.A.V., Maestro, A., Alveirinho Dias, J.M., 2001. Seismic stacking pattern of the Faro-Albufeira contourite system (Gulf of Cadiz): a Quaternary record of paleoceanographic and tectonic influences. Mar. Geophys. Res. 22 (5–6), 487–508. https://doi.org/10.1023/A:1016355801344.

Lutjeharms, J.R.E., 2006. The Agulhas Current. vol. 329 Springer-Verlag Berlin Heidelberg978-3-540-37212-7.

Maas, L.R.M., Aguiar-González, B., Ponsoni, L., 2018. Deep-Ocean tides in the South-west Indian Ocean: Comparing deep-sea pressure to satellite data. In: Velarde, M., Tarakanov, R., Marchenko, A. (Eds.), The Ocean in Motion. Springer Oceanography. *Springer*, pp. 147–182. https://doi.org/10.1007/978-3-319-71934-4_12.

Magalhaes, J.M., da Silva, J.C.B., New, A.L., 2014. Internal solitary waves system in the Mozambique channel. In: Barale, V., Gade, M. (Eds.), Remote Sensing of the African Seas. Springer, Dordrecht, pp. 263–284. https://doi.org/10.1007/978-94-017-8008-7_14.

Manders, A.M.M., Maas, L.R.M., Gerkema, T., 2004. Observations of internal tides in the Mozambique Channel. J. Geophys. Res. 109, C12. https://doi.org/10.1029/2003JC002187.

Manley, P.L., Flood, R.D., 1993. Project MUDWAVES. Deep Sea Res. II 40, 851–857. https://doi.org/10.1016/0967-0645(93)90037-N.

Martin, A.K., 1981. The influence of the Agulhas current on the physiographic development of the northernmost Natal Valley (S.W. Indian Ocean). Mar. Geol. 39 (3–4), 259–276. https://doi.org/10.1016/0025-3227(81)90075-x.

McCave, I.N., 2009. Nepheloid layers. In: Steele, J.H., Thorpe, S.A., Turekian, K.K. (Eds.), Encyclopedia of Ocean Sciences, 2nd ed. Academic Press, London, pp. 8–18. 978-0-12-374473-9. https://doi.org/10.1016/B978-012374473-9.00671-8.

McCave, I.N., Tucholke, B.E., 1986. Deep current controlled sedimentation in the western North Atlantic. In: Vogt, P.R., Tucholke, B.E. (Eds.), The Western North Atlantic Region. vol. M. Geology of North America, pp. 451–468. https://doi.org/10.1130/DNAG-GNA-M.451.

McElhinny, M.W., 1970. Formation of the Indian Ocean. Nature 228, 977–979. https://doi.org/10.1038/228977a0.

McKenzie, D., Sclater, J.G., 1971. The evolution of the Indian Ocean since the late Cretaceous. Geophys. J. Int. 24 (5), 437–528. https://doi.org/10.1111/j.1365-246X.1971.tb02190.x.

Milliman, J.D., 1981. Transfer of river-borne material to the oceans. In: Martin, J.M., Burton, J.D., Eisma, D. (Eds.), River Inputs to Ocean Systems. UNESCO, Paris, pp. 5–12.

Miramontes, E., Cattaneo, A., Jouet, G., Thereau, E., Thomas, Y., Rovere, M., Cauquil, E., Trincardi, F., 2016. The pianosa contourite depositional system (northern Tyrrhenian Sea): drift morphology and plio-quaternary stratigraphic evolution. Mar. Geol. 378, 20–42. https://doi.org/10.1016/j.margeo.2015.11.004.

Mosher, D.C., Campbell, D.C., Gardner, J.V., Piper, J.W., Chavtor, J.D., Rebesco, M., 2017. The role of deep-water sedimentary processes in shaping a continental margin: The Northwest Atlantic. Mar. Geol. 393, 245–259. https://doi.org/10.1016/j.margeo.2017.08.018.

Mougenot, D., Recq, M., Virlogeux, P., Lepvrier, C., 1986. Seaward extension of the East African Rift. Nature 321, 599–603. https://doi.org/10.1038/321599a0.

Niemi, T.M., Ben-avraham, Z., Hartnady, C.J.H., Reznikov, M., 2000. Post-Eocene seismic stratigraphy of the deep ocean basin adjacent to the southeast African continental margin: a record of geostrophic bottom current systems. Mar. Geol. 162 (2–4), 237–258. https://doi.org/10.1016/S0025-3227(99)00062-6.

Orsia, A.H., Johnsonb, G.C., Bullisterb, J.L., 1999. Circulation, mixing, and production of Antarctic bottom water. Prog. Oceanogr. 43 (1), 55–109. https://doi.org/10.1016/S0079-6611(99)00004-X.

Peeters, F.J.C., Acheson, R., Brummer, G.J.A., de Ruijter, W.P.M., Schneider, R.R., Ganssen, G.M., Ufkes, E., Kroon, D., 2004. Vigorous exchange between the Indian and Atlantic Oceans at the end of the past five glacial periods. Nature 430 (7000), 661–665. https://doi.org/10.1038/nature02785.

Pena, L.D., Goldstein, S.L., 2014. Thermohaline circulation crisis and impacts during the mid-Pleistocene transition. Science 345 (6194), 318–322. https://doi.org/10.1126/science.1249770.

Petrick, B.F., McClymont, E.L., Marret, F., van der Meer, M.T.J., 2015. Changing surface water conditions for the last 500 ka in the southeast Atlantic: implications for variable influences of Agulhas leakage and Benguela upwelling. Paleoceanography 30 (9), 1153–1167. https://doi.org/10.1002/2015PA002787.

Pomar, L., Morsilli, M., Hallock, P., Bádenas, B., 2012. Internal waves, an underexplored source of turbulence events in the sedimentary record. Earth Sci. Rev. 111 (1–2), 56–81. https://doi.org/10.1016/j.earscirev.2011.12.005.

Preu, B., Spieß, V., Schwenk, T., Schneider, R., 2011. Evidence for current-controlled sedimentation along the southern Mozambique continental margin since Early Miocene times. Geo Mar. Lett. 31 (5–6), 427–435. https://doi.org/10.1007/s00367-011-0238-y.

Preu, B., Hernández-Molina, F.J., Violante, R., Piola, A.R., Paterlini, C.M., Schwenk, T., Spiess, V., 2013. Morphosedimentary and hydrographic features of the northern Argentine margin: the interplay between erosive, depositional and gravitational processes and its conceptual implications. Deep-Sea Res. Part I: Oceanography Research Papers 75, 157–174. https://doi.org/10.1016/j.dsr.2012.12.013.

Puig, P., Palanques, A., Guillén, J., El Khatab, M., 2004. Role of internal waves in the generation of nepheloid layers on the northwestern Alboran slope: implications for continental margin shaping. J. Geophys. Res. Ocean. 109 C9. https://doi.org/10.1029/2004JC002394.

Read, J.F., Pollard, R.T., 1999. Deep inflow into the Mozambique basin. J. Geophys. Res. Ocean. 104 (C2), 3075–3090. https://doi.org/10.1029/1998JC900078.

Rebesco, M., 2005. Contourites. In: Selley, R.C., Cocks, L.R.M., Plimer, I.R. (Eds.), Encyclopedia of Geology. Elsevier, Oxford, pp. 513–527 978-0-12-369396-9.

Rebesco, M., Camerlenghi, A., 2008. Contourites. Developments in Sedimentology. vol. 60. Elsevier Science, Amsterdam, pp. 688 978-0-444-52998-5.

Rebesco, M., Stow, D., 2001. Seismic expression of contourites and related deposits: a preface. Mar. Geophys. Res. 22 (5–6), 303–308. https://doi.org/10.1023/A:1016316913639.

Rebesco, M., Hernández-Molina, F.J., van Rooij, D., Wåhlin, A., 2014. Contourites and associated sediments controlled by deep-water circulation processes: state-of-the-art and future considerations. Mar. Geol. 352, 111–154. https://doi.org/10.1016/j.margeo.2014.03.011.

Ridderinkhof, H., de Ruijter, W.P.M., 2003. Moored current observations in the Mozambique Channel. Deep-Sea Res. Part II Top. Stud. Oceanogr. 50, 12–13. 1933–1955. https://doi.org/10.1016/S0967-0645(03)00041-9.

Said, A., Moder, C., Clark, S., Ghorbal, B., 2015. Cretaceous-Cenozoic sedimentary budgets of the Southern Mozambique Basin: implications for uplift history of the South African Plateau. J. Afr. Earth Sci. 109, 1–10. https://doi.org/10.1016/j.jafrearsci.2015.05.007.

Sansom, P., 2018. Hybrid turbidite-contourite systems of the Tanzanian margin. Petrol. Geosci. https://doi.org/10.1144/petgeo2018-044.
Schlitzer, R., 2013. Ocean Data View. http://odv.awi.de.
Schlüter, P., Uenzelmann-Neben, G., 2008. Indications for bottom current activity since Eocene times: the climate and ocean gateway archive of the Transkei Basin, South Africa. Glob. Planet. Chang. 60 (3–4), 416–428. https://doi.org/10.1016/j.gloplacha.2007.07.002.
Schott, F.A., McCreary Jr., J.P., 2001. The monsoon circulation of the Indian Ocean. Prog. Oceanogr. 51 (1), 1–123. https://doi.org/10.1016/S0079-6611(01)00083-0.
Schouten, M.W., de Ruijter, W.P.M., van Leeuwen, P.J., Ridderinkhof, H., 2003. Eddies and variability in the Mozambique channel. Deep Sea Res. Part II Top. Stud. Oceanogr. 50, 12–13. https://doi.org/10.1016/S0967-0645(03)00042-0 1987-2003.
Schulz, H., Lückge, A., Emeis, K., Mackensen, A., 2011. Variability of Holocene to Late Pleistocene Zambezi riverine sedimentation at the upper continental slope off Mozambique, 15°–21°S. Mar. Geol. 286 (1–4), 21–34. https://doi.org/10.1016/j.margeo.2011.05.003.
Shanmugam, G., 2013. Modern internal waves and internal tides along oceanic pycnoclines: challenges and implications for ancient deep-marine baroclinic sands. AAPG (Am. Assoc. Pet. Geol.) Bull. 97 (5), 799–843. https://doi.org/10.1306/10171212101.
Shanmugam, G., 2014. Modern internal waves and internal tides along oceanic pycnoclines: challenges and implications for ancient deep-marine baroclinic sands: reply. AAPG (Am. Assoc. Pet. Geol.) Bull. 98 (4), 858–879. https://doi.org/10.1306/09111313115.
Shchepetkin, A.F., McWilliams, J.C., 2005. The regional oceanic modeling system (ROMS): a split-explicit, free-surface, topography-following-coordinate oceanic model. Ocean Model. 9, 347–404. https://doi.org/10.1016/j.ocemod.2004.08.002.
Shepard, F.P., 1963. Submarine Geology, 2nd Edition. Harper and Row, New York, pp. 557.
Sinha, M.C., Louden, K.E., Parsons, B., 1981. The crustal structure of the Madagascar Ridge. Geophys. J. Int. 66 (2), 351–377. https://doi.org/10.1111/j.1365-246X.1981.tb05960.x.
Stow, D.A.V., 1994. Deep sea processes of sediment transport and deposition. In: Kenneth, P. (Ed.), Sediment Transport and Depositional Processes. Blackwell Scientific Publications, Oxford, pp. 257–291 0-632-03112-3.
Stow, D.A.V., Faugères, J.C., Howe, J.A., Pudsey, C.J., Viana, A., 2002. Contourites, bottom currents and deep-sea sediment drifts: current state-of-the-art. In: Stow, D.A.V., Pudsey, C.J., Howe, J.A., Faugères, J.C., Viana, A.R. (Eds.), Deep-Water Contourite Systems: Modern Drifts and Ancient Series, Seismic and Sedimentary Characteristics. vol. 22. Geological Society of London, Memoirs, pp. 7–20. https://doi.org/10.1144/GSL.MEM.2002.022.01.02.
Stow, D.A.V., Hernández-Molina, F.J., Llave, E., Sayago, M., Díaz del Río, V., Branson, A., 2009. Bedform-velocity matrix: the estimation of bottom current velocity from bedform observations. Geology 37 (4), 327–330. https://doi.org/10.1130/G25259A.1.
Swart, N.C., Lutjeharms, J.R.E., Ridderinkhof, H., de Ruijter, W.P.M., 2010. Observed characteristics of Mozambique Channel eddies. J. Geophys. Res. 115, 1–14. https://doi.org/10.1029/2009JC005875.
Talley, L., 1996. Antarctic intermediate water in the South Atlantic. In: Wefer, G., Berger, W.H., Siedler, G., Webb, D.J. (Eds.), The South Atlantic: Present and Past Circulation. Springer, Berlin, Heidelberg, pp. 219–238. https://doi.org/10.1007/978-3-642-80353-6_11.
Ternon, J.F., Roberts, M.J., Morris, T., Hancke, L., Backeberg, B., 2014. In situ measured current structures of the eddy field in the Mozambique Channel. Deep Sea Res. Part II Top. Stud. Oceanogr. 100, 10–26. https://doi.org/10.1016/j.dsr2.2013.10.013.
Toole, J.M., Warren, B.A., 1993. A hydrographic section across the subtropical South Indian Ocean. Deep-Sea Res. Part I Oceanogr. Res. Pap. 40 (10), 1973–2019. https://doi.org/10.1016/0967-0637(93)90042-2.
Tucholke, B.E., Embley, R.W., 1984. Cenozoic regional erosion of the Abyssal Sea floor off South Africa. In: Schlee, J.S. (Ed.), Interregional Unconformities and Hydrocarbon Accumulation. vol. 36. AAPG Memoir, pp. 145–164. https://doi.org/10.1306/M36440C11.
Uenzelmann-Neben, G., 2001. Seismic characteristics of sediment drifts: An example from the Agulhas Plateau, southwest Indian Ocean. Mar. Geophys. Res. 22 (5–6), 323–343. https://doi.org/10.1023/A:1016391314547.
Uenzelmann-Neben, G., Huhn, K., 2009. Sedimentary deposits on the southern South African continental margin: Slumping versus non deposition or erosion by oceanic currents? Mar. Geol. 266, 6–79. https://doi.org/10.2113/gssajg.114.3-4.449.
Uenzelmann-Neben, G., Watkeys, M.K., Kretzinger, W., Frank, M., Heuer, L., 2011. Paleoceanogrpahic interpretation of a seismic profile from the southern Mozambique ridge, Southwestern Indian Ocean. S. Afr. J. Geol. 114 (3–4), 449–458. https://doi.org/10.2113/gssajg.114.3-4.449.
Ullgren, J.E., van Aken, H.M., Ridderinkohof, H., de Ruijter, W.P.M., 2012. The hydrography of the Mozambique Channel from six years of continuous temperature, salinity, and velocity observations. Deep Sea Res. Oceanogr. Res. Pap. 69, 36–50. https://doi.org/10.1016/j.dsr.2012.07.003.
van Aken, H.M., Ridderinkhof, H., de Ruijter, W.P.M., 2004. North Atlantic deep water in the south-western Indian Ocean. Deep Sea Res. Oceanogr. Res. Pap. 51 (6), 755–776. https://doi.org/10.1016/j.dsr.2004.01.008.
van Haren, H., Gostiaux, L., 2011. Large internal wave advection in very weakly stratified deep Mediterranean waters. Geophys. Res. Lett. 38, 22. https://doi.org/10.1029/2011GL049707.
Viana, A.R., Almeida Jr., W., Nunes, M.C.V., Bulhões, E.M., 2007. The Economic Importance of Contourites. vol. 276. Geological Society, London, Special Publication, pp. 1–23. https://doi.org/10.1144/GSL.SP.2007.276.01.01.
Walford, H.L., White, N.J., Sydow, J.C., 2005. Solid sediment load history of the Zambezi Delta. Earth Planet. Sci. Lett. 238 (1–2), 49–63. https://doi.org/10.1016/j.epsl.2005.07.014.
Watkeys, M.K., Sokoutis, D., 1998. Transtension in southeastern Africa associated with Gondwana break-up. Special Publications. Geol. Soc. Lon. 135, 203–214. https://doi.org/10.1144/GSL.SP.1998.135.01.13.
Weatherall, P., Marks, K.M., Jakobsson, M., Schmitt, T., Tani, S., Arndt, J.E., Rovere, M., Chayes, D., Ferrini, V., Wigley, R., 2015. A new digital bathymetric model of the world's oceans. Earth and Space Sci. 2 (8), 331–345. http://doi.org/10.1002/2015EA000107.
Wiles, E., Green, A., Watkeys, M., Jokat, W., Krocker, R., 2014. A new pathway for Deep water exchange between the Natal Valley and Mozambique Basin? Geo Mar. Lett. 34 (6), 525–540. https://doi.org/10.1007/s00367-014-0383-1.
Wiles, E., Green, A.N., Watkeys, M.K., Jokat, W., 2017. Zambezi continental margin: compartmentalized sediment transfer routes to the abyssal Mozambique Channel. Mar. Geophys. Res. 38 (3), 227–240. https://doi.org/10.1007/s11001-016-9301-4.
Wilson, A.M., Raine, R., Mohn, C., White, M., 2015. Nepheloid layer distribution in the Whittard Canyon, NE Atlantic margin. Mar. Geol. 367, 130–142. https://doi.org/10.1016/j.margeo.2015.06.002.
Xie, J., He, Y., Chen, Z., Xu, J., Cai, S., 2015. Simulations of internal solitary wave interactions with mesoscale eddies in the northeastern South China Sea. J. Phys. Oceanogr. 45 (12), 2959–2978. https://doi.org/10.1175/JPO-D-15-0029.1.